

Cross-correlating *WMAP5* with 1.5 million LRGs: a new test for the ISW effect

U. Sawangwit^{1*}, T. Shanks^{1†}, R.D. Cannon², S.M. Croom³, Nicholas P. Ross^{1,4}
and D.A. Wake^{1,5}

¹*Physics Department, University of Durham, South Road, Durham, DH1 3LE, UK*

²*Anglo-Australian Observatory, PO Box 296, Epping, NSW 1710, Australia*

³*School of Physics, University of Sydney, NSW 2006, Australia*

⁴*Department of Astronomy and Astrophysics, The Pennsylvania State University, University Park, PA 16802, USA*

⁵*Department of Astronomy, Yale University, CT 06520, USA*

Accepted 2009 November 16. Received 2009 November 06; in original form 2009 May 25

ABSTRACT

We present the cross-correlation of the density map of Luminous Red Galaxies (LRGs) and the temperature fluctuation in the Cosmic Microwave Background (CMB) as measured by the five-year Wilkinson Microwave Anisotropy Probe (*WMAP*) observations. The LRG samples were extracted from imaging data of the Sloan Digital Sky Survey (SDSS) Data Release 5 (DR5) based on two previous spectroscopic redshift surveys, the SDSS–LRG and the 2dF–SDSS LRG and QSO (2SLAQ) surveys designed to have average redshifts of $z \approx 0.35$ and $z \approx 0.55$. In addition we have added a higher–redshift photometric LRG sample based on the selection of the AAOmega LRG redshift survey at $z \approx 0.7$. The total LRG sample thus comprises 1.5 million galaxies, sampling a redshift range of $0.2 < z < 0.9$ over ≈ 7600 square degrees of the sky, probing a total cosmic volume of $\approx 5.5h^{-3} \text{ Gpc}^3$.

First, we find that the new LRG sample at $z \approx 0.7$ shows very little positive evidence for the Integrated Sachs-Wolfe (ISW) effect. Indeed, the cross-correlation is negative out to $\approx 1^\circ$. The standard Λ CDM model is rejected at $\approx 2\text{--}3\%$ significance by the new LRG data. We then analyse the previous samples at $z \approx 0.35$ and $z \approx 0.55$. As found by other authors, these results appear consistent with the standard ISW model, although the statistical significance remains marginal. We also reproduce the same result for the magnitude limited SDSS galaxy samples of Cabré et al. (2006). Taking the $z \approx 0.35$ and $z \approx 0.55$ LRG results in combination with the new $z \approx 0.7$ sample, the overall result is now more consistent with a null detection than with the standard Λ CDM model prediction.

We then performed a new test on the robustness of the LRG ISW detections at $z \approx 0.35$ and $z \approx 0.55$. We made 8 rotations through 360° of the CMB maps with respect to the LRG samples around the galactic pole. We find that in both cases there are stronger effects at angles other than zero. This implies that the $z \approx 0.35$ and $z \approx 0.55$ ISW detections may still be subject to systematic errors which combined with the known sizeable statistical errors may leave the $z \approx 0.35$ and $z \approx 0.55$ ISW detections looking unreliable. We have further made the rotation test on several other samples where ISW detections have been claimed and find that they also show peaks when rotated. We conclude that in the samples we have tested the ISW effect may be absent and we argue that this result may not be in contradiction with previous results.

Key words: cosmology: observations – cosmic microwave background – large-scale structure of Universe.

1 INTRODUCTION

Many observations now suggest that we live in a spatially flat, dark energy dominated Universe (e.g. Perlmutter et al.

* E-mail: utane.sawangwit@durham.ac.uk

† E-mail: tom.shanks@durham.ac.uk

1999; Cole et al. 2005; Tegmark et al. 2006; Riess et al. 2007; Dunkley et al. 2009). In such a cosmology, positive correlation between the CMB and large-scale-structure (LSS) is expected due to the decaying gravitational potential (Sachs & Wolfe 1967). The deviation of the CMB temperature in the vicinity of LSS is caused by the non-vanishing difference in the energy gained and lost by the CMB photons as they traverse a region of over- or under-density. By integrating across all the potential wells along the line of sight from the surface of last scattering, the primordial fluctuations in the CMB are modified by this effect. This secondary anisotropy of the CMB is called the Integrated Sachs–Wolfe (ISW) effect and sometimes known as the late-time ISW effect since the dominance of dark energy in the cosmic energy budget at the present epoch is believed to be responsible for the current accelerating expansion and hence the decaying gravitational potential. For a spatially flat Universe, a detection of the Integrated Sachs–Wolfe (ISW) effect would provide direct dynamical evidence of the accelerating expansion unlike the geometrical measurement inferred from standard candles such as the SNIa.

The SNIa results coupled with the CMB evidence that the Universe is nearly flat, suggests there exists an exotic form of energy with negative pressure. The exact nature of this so-called dark energy is not yet known but it already entails many serious problems. Foremost amongst them are the fine-tuning problem and the cosmic coincidence problem (e.g. Carroll 2001; Peebles & Ratra 2003).

The ISW signal in the CMB–galaxy cross-correlation is very small, generally less than one μK , and very difficult to detect. Previous ISW detections generally have less than 3σ statistical significance. These include the studies of Fosalba et al. (2003), Padmanabhan et al. (2005) and Cabré et al. (2006) who used SDSS galaxies in both photo- z and magnitude limited samples and the WMAP3 dataset. Other authors have used X-ray sources (Boughn & Crittenden 2004) and NVSS radio sources (Nolta et al. 2004). Of these, it seems that up to now the most significant detection of the ISW effect comes from the NVSS radio sources at 2.3σ . Other authors (eg Giannantonio et al. 2008 and Ho et al. 2008) have made compilations of the other results and claimed up to 4σ ISW detections in terms of the overall significance. The only other claims of ISW detections at high significance are the methods that reduced the galaxy samples to focus only on regions of high or low underdensity. In particular, Granett et al. (2008) cross-correlated the positions of ≈ 100 superclusters and voids in the MegaZ–LRG (Collister et al. 2007) sample and McEwen et al. (2007) employed a similar wavelets method using radio sources from NVSS.

Here we shall search for the ISW effect by using samples of Luminous Red Galaxies (LRGs) from the SDSS DR5 dataset. LRGs are the most luminous stellar systems in the Universe, residing in the most massive dark matter haloes. Having formed most of their stars much earlier and over short period of time, the objects appear red with reasonably uniform spectral energy distributions therefore these galaxy samples can be selected homogeneously and observed out to greater distance (or lookback time). Moreover, being massive means that the LRGs are also a highly biased tracer of the LSS (e.g. Ross et al. 2007, Wake et al. 2008). The selection techniques for $z < 0.6$ LRG samples have been well

established in the literature. Many LSS studies have been carried out using these LRG samples including the claimed detections of the ISW effect (e.g. Cabré et al. 2006). The recent spectroscopic survey by Ross et al. (2008) has shown that it is possible to extend the selection technique and hence the LRG sample out to $z \approx 1$. Applying this tested algorithm to the entire SDSS imaging significantly increases the effective volume and makes these LRGs ideal probes of large-scale structure.

Our main goal is to detect the ISW signal in the CMB by cross-correlating WMAP5 map with the new $\bar{z} \approx 0.7$ LRG sample and to test the detection of the ISW effect caused by the LRGs at lower redshift ($\bar{z} \approx 0.35, 0.55$) as claimed by a number of authors (e.g. Padmanabhan et al. 2005, Cabré et al. 2006). These studies used the LRG candidates extracted from the SDSS DR3 or DR4 whilst we are using DR5, ≈ 50 per cent and 20 per cent increase in the area coverage, respectively. The larger sky coverage should provide a statistical advantage over the previous studies. Our new higher redshift LRG sample should also provide a chance to constrain the evolution if such an effect is indeed detected. Moreover, a recent study by Douspis et al. (2008) suggests that the ISW signal-to-noise can be optimised if the large-scale tracer probes out to a median redshift of 0.8 but there is no further improvement after a redshift of unity. The claim appears to be supported by the cross-correlation analysis of Giannantonio et al. (2008) in which the signal-to-noise of the ISW detection from the 2 Micron All Sky Survey (2MASS; Jarrett et al. 2000) is ≈ 4 –6 times smaller than from the NRAO VLA Sky Survey (NVSS; Condon et al. 1998) where $\bar{z} \approx 0.1$ and 0.8 respectively, despite the fact that the two surveys have similar sky coverage and sky density ($N_{\text{NVSS}} \approx 2N_{\text{2MASS}}$). If this is true then our higher redshift LRG should be more sensitive to the ISW signal and will provide even higher significance of detection than previous studies using the LRGs which currently reach $\approx 2\sigma$ significance at best. The new sample therefore presents a fresh opportunity to test one of the most crucial manifestations of the accelerating expansion, obtaining independent confirmation of the geometrical inference of the SNIa result if detected and a challenge to the current standard picture of the Universe otherwise.

The layout of this paper is as follows. We present the data in §2. We then outline the theoretical prediction and cross-correlation technique employed in this study in §3 and §4, respectively. The results and a range of analyses performed to ensure their robustness are given in §5 and §6. The additional sky rotation tests performed on our dataset and selections of previously claimed ISW detections are reported in §7. We then present the discussion and conclusion of our studies in §8 and §9. Throughout this study (unless otherwise stated), we assume a standard ΛCDM cosmology with $\Omega_{\Lambda} = 0.7$, $\Omega_{\text{m}} = 0.3$, $f_{\text{baryon}} = 0.167$, $\sigma_8 = 0.8$ and $H_0 = 100h \text{ km s}^{-1} \text{ Mpc}^{-1}$ ($h = 0.7$ where necessary).

2 DATA

2.1 CMB Temperature Map- WMAP5

The CMB temperature maps used here are taken from the WMAP five-year data release (Hinshaw et al. 2009).

The data products are publicly available¹ in Hierarchical Equal Area isoLatitude Pixelisation (HEALPix, Górski et al. 2005) format. Although the *WMAP* observes in five frequency bands, we choose to use only the three highest-frequency bands, namely, *W* at 94 GHz, *V* at 61 GHz and *Q* at 41 GHz as the CMB anisotropy in these ranges are less susceptible to a contamination from the foreground anisotropy (i.e. synchrotron and free-free emission) than the lower frequency counterparts. This enable us to test for any wavelength dependence in the CMB-galaxy cross-correlation where one expects the ISW signal to be achromatic. However, we shall concentrate our analysis mainly on the *W* band due to its relatively high resolution compared to the other bands, 12.6 FWHM compared to 19.8 for *V* and 29.4 for *Q* band. Despite the fact that the *V* band has lower noise than the *W* band (hence often the band of choice for this type of analysis), we do not observe any major difference in either the cross-correlation results or their statistical errors (see Fig. 3). We also use the Internal Linear Combination (ILC, Gold et al. 2009) to further check our results, although it should be noted that, according to the *WMAP* team, there could be a significant structure in the bias correction map at scales smaller than $\approx 10^\circ$ (Limon et al. 2008).

We shall use the temperature maps at a resolution of $N_{\text{side}}=512$ (res=9) which for the whole sky, contains 3 145 728 pixels each with an area of ≈ 49 arcmin². The foreground-contaminated regions of the sky, mainly in Galactic Plane and Magellanic Cloud including extragalactic point sources, are excluded using a combination of ‘Extended temperature analysis mask’ (KQ75, Gold et al. 2009) and ‘Point source catalogue mask’ (Wright et al. 2009). After applying the masks, we are left with 2 239 993 pixels (≈ 70 per cent). The maps contain thermodynamic temperatures with the dipole contribution subtracted from the data by the *WMAP* team (Hinshaw et al. 2009).

2.2 Luminous Red Galaxies

The Luminous Red Galaxy (LRG) photometric samples are extracted from the SDSS DR5 (Adelman-McCarthy et al. 2007) imaging data based on three LRG spectroscopic redshift surveys whose median redshifts are $\approx 0.35, 0.55$ and 0.7 (Eisenstein et al. 2001; Cannon et al. 2006; Ross et al. 2008). In essence, these surveys utilised a crude but effective determination of photometric redshift (photo-*z*), owing to the strong 4000 Å break of a typical E/S0 galaxy spectral energy distribution (SED). As the break is redshifted through the SDSS *u, g, r, i,* and *z* bandpasses, its colour-colour track exhibits a distinctive turning point at various redshifts for different colour pairs. Moreover, their uniform SEDs ensure that they have an extremely tight locus in the colour space. This allows the potential LRGs in the desired redshift ranges to be selected uniformly using their locations on the colour-colour plane coupled with the luminosity threshold set by the appropriate magnitude limit.

These simple methods have been proven to be highly effective in selecting the intrinsically luminous early-type galaxies in the targeted redshift ranges as demonstrated

Table 1. Summary of the LRG samples used in the cross-correlation analyses.

Sample	\bar{z}	Number	Sky density (deg ⁻²)	Magnitude (AB)
SDSS	0.35	106 699	≈ 13	$17.5 \leq r < 19.5$
2SLAQ	0.55	655 775	≈ 85	$17.5 < i < 19.8$
AAΩ	0.68	800 346	≈ 105	$19.8 < i \leq 20.5$

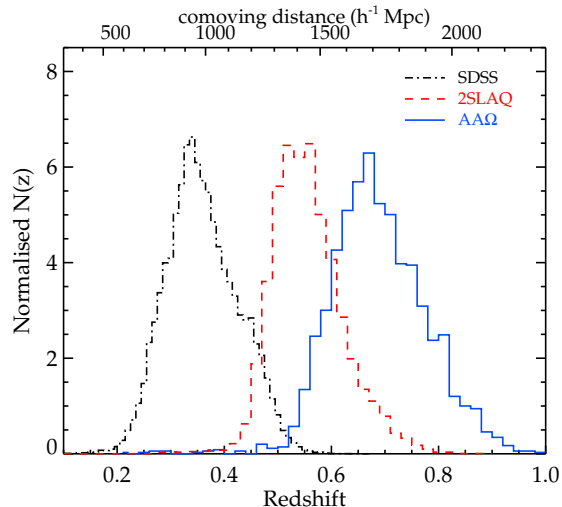


Figure 1. Redshift distribution of the three LRG samples inferred from the redshift surveys used in their selections.

by the SDSS–LRG, 2SLAQ and AAT–AAΩ redshift surveys (Eisenstein et al. 2001; Cannon et al. 2006; Ross et al. 2008). Although the LRG photo-*z* in these redshift ranges can be estimated quite accurately (Padmanabhan et al. 2007; Collister et al. 2007), we decided to base our study on the colour–magnitude cuts because a well defined photo-*z* error distribution is needed for the deconvolution to recover the real redshift distribution and could bias the analyses of the results. The colour-magnitude cut techniques used in the above spectroscopic surveys, applied to the entire SDSS DR5 dataset (only Northern Galactic Cap), results in ≈ 1.5 million LRG candidates and the redshift distribution of the survey is assumed for the corresponding photometric sample. The outlines of the selection algorithms with the emphasis on any differences in our criteria to that of the spectroscopic surveys are given below (readers are referred to Eisenstein et al. 2001; Cannon et al. 2006; Ross et al. 2008 for the detailed descriptions of the selection criteria). The number-redshift relations, $N(z)$, (shown in Fig. 1) used in the model predictions have been calibrated to include those differences. The summary of the three LRG samples is given in Table 1.

For the following sections, all magnitudes and colours are given in SDSS *AB* system (unless otherwise stated) and are corrected for galactic extinction using the galactic dust map of Schlegel, Finkbeiner & Davis (1998).

¹ <http://lambda.gsfc.nasa.gov/>

2.2.1 SDSS LRG

The low redshift (median $z \approx 0.35$) LRG candidates are selected on the basis of their colours and magnitudes following the ongoing SDSS-LRG spectroscopic survey (Eisenstein et al. 2001, E01 hereafter) which will contain more than 100 000 spectra and cover over $1h^{-3} \text{ Gpc}^3$ when completed. The survey is designed to be approximately volume-limited up to $z \approx 0.4$. The targets are selected using $g - r$ and $r - i$ colour cuts with the magnitude limit, $r_{\text{petro}} < 19.5$. Two sets of selection criteria (*Cut I* and *Cut II* in E01) are used to extract LRGs in two different (but slightly overlapped) regions of the gri colour space, separated by the turn-over of the gri colour track at $z \approx 0.4$.

In addition to the criteria of E01, we also apply restriction on the bright limit in the r -band, i.e. $r_{\text{petro}} \geq 17.5$. This is mainly because *Cut I* is too permissive and allows underluminous objects to enter the sample below redshift 0.2 and by imposing the bright limit, we restrict the sample to only $z \gtrsim 0.2$. The choice of $r_{\text{petro}} \geq 17.5$ merits a brief explanation. The redshift-dependent luminosity threshold is implemented by one of the selection rules, $r_{\text{petro}} < 13.1 + c_{\parallel}/0.3$ (Eq. 4 in E01), where $c_{\parallel} \approx g - r$ at $z \approx 0.2$ corresponds to $g - r \approx 1.3$ on the gri colour-colour track. This has been empirically confirmed to work sufficiently well using the spectroscopic sample, with only a few objects having $r_{\text{petro}} < 17.5$ at $z > 0.2$ and vice versa.

The LRG sample described above is then extracted from the SDSS DR5 imaging database using the SQL query by setting the flag PRIMTARGET to GALAXY_RED. This yields a catalogue of approximately 200 000 objects which after applying the bright flux cut mentioned above, becomes 106 699 objects with the sky surface density of $\approx 13 \text{ deg}^{-2}$. The average redshift of the LRG candidates as inferred from the spectroscopic sample of $\approx 60 000$ SDSS-LRG is $z = 0.35 \pm 0.06$.

2.2.2 2SLAQ LRG

The 2dF-SDSS LRG and Quasar Survey (2SLAQ) is the spectroscopic follow-up of the intermediate redshift ($z > 0.4$) LRGs from photometric data of the SDSS survey using the 2-degree Field (2dF) instrument on the 3.9-m Anglo-Australian Telescope (AAT). The survey was completed in 2006 and contains approximately 13 000 spectroscopically confirmed LRGs with $0.4 < z < 0.8$ in two equatorial strips covering $\approx 180 \text{ deg}^2$ (Cannon et al. 2006, and references therein). The primary and secondary sample of the survey (*Sample 8* and *9*, respectively) were selected using the SDSS $g - r$ versus $r - i$ colours in conjunction with the ‘de Vaucouleurs’ i -band magnitude, ($17.5 < i_{\text{dev}} < 19.8$). The colour cuts are similar to the *Cut II* used by E01 which targets the objects lie above the turning point of the early-type galaxy track in gri colour space. The turning point is caused by the 4000 Å break moving into the r -band at $z \approx 0.4$, making $r - i$ colour increase rapidly whereas $g - r$ remains nearly constant at 1.6–1.7 mag until $z \approx 0.7$.

In order to qualify as 2SLAQ LRG candidates, objects are required to have $d_{\perp} \geq 0.65$ for the primary sample and $0.55 \leq d_{\perp} < 0.65$ for the secondary sample, where $d_{\perp} = (r - i) - (g - r)/8.0$. We shall only use the LRG candidates extracted following the primary sample cut, de-

signed to target higher redshift candidates than the secondary sample. We also utilise the star-galaxy separation criterion used by the 2SLAQ survey which has been proven to be very effective and the stellar contamination in the LRG sample is only 5 per cent. The primary sample contains 67 per cent of all 2SLAQ LRGs and has an average redshift of $z = 0.55 \pm 0.06$. Applying the primary target selection, including the star-galaxy separation criteria, on the DR5 ‘best’ imaging database in the NGC, a sample of 655 775 photometrically classified LRGs is returned. Objects with BRIGHT or SATURATED or BLENDED but not DEBLENDED flags are not included in our sample.

2.2.3 AAΩ LRG

Our new high redshift LRG sample is based on the AAT-AAΩ LRG Pilot run (Ross et al. 2008, and references therein), using the 2dF instrument on the AAT. The survey was carried out as a ‘Proof of Concept’ for a large LRG redshift survey, VST-AAΩ *ATLAS* survey. It was designed to target potential LRGs out to $z \approx 1.0$ with the average redshift of 0.7. Three different sets of selection criteria were employed in selecting the targets in order to test the AAΩ spectrograph’s ability to obtain reliable redshift with the minimum exposure time in average conditions. They observed over $\approx 10 \text{ deg}^2$ in three 2dF fields and the survey contains 1270 unique galaxy spectra with 804 high-confidence LRG redshifts.

The selection rules used here follow the colour-magnitude cuts which utilise the riz colour plane and the ‘de Vaucouleurs’ i -band magnitude. This selection forms the main part of the survey. In summary, the colour cuts exploit the upturn of the early-type galaxy track similar to that used by 2SLAQ and SDSS LRGs survey in selecting $z > 0.4$ LRGs with gri colours. But in the riz colour space, the upturn occurs between redshift 0.6 and 0.7 as the 4000 Å feature moves into the i band hence makes it ideal for selecting potential LRG targets for the intended redshift range. The star-galaxy separation procedure uses the z -band photometry, akin to the method which has proven effective in the SDSS- and 2SLAQ-LRG redshift survey where a similar procedure were performed using the i -band photometry. Our star-galaxy separation algorithm only loses genuine LRGs at a sub-percent level and leaves ≈ 16 per cent stellar contamination in the sample.

The riz selection has been proven to work reasonably well, resulting in the sample having average redshift $z = 0.68 \pm 0.07$. The redshift distribution is further confirmed by the ongoing AAT-AAΩ LRG project, a downsized version of the VST-AAΩ *ATLAS* survey, designed to observe several thousands LRG redshifts for photo- z calibration and clustering evolution study. The $N(z)$ used in the model prediction of ISW signal comes from ≈ 2000 AAΩ LRG redshifts taken during a run in June 2008 (Sawangwit et al. 2009, in prep.) as well as those from Ross et al. (2008).

The SDSS DR5 ‘best’ imaging database contains 800 346 photometric objects that satisfied the AAΩ LRG selection rules including the necessary star-galaxy separation performed in the z -band. As with the 2SLAQ LRG sample, objects with BRIGHT or SATURATED or BLENDED but not DEBLENDED flags are discarded from our sample.

3 THEORETICAL PREDICTION

The secondary CMB anisotropy caused by the time-varying gravitational potential, Φ , is known as the Integrated Sachs-Wolfe (ISW) effect. As the CMB photons traverse such regions, the temperature perturbation associated with the time dependent potential is given by

$$\delta_T^{\text{ISW}}(\hat{\mathbf{n}}) \equiv \frac{\Delta_T^{\text{ISW}}(\hat{\mathbf{n}})}{T_0} = -2 \int_0^{z_{\text{LS}}} dz \frac{1}{c^2} \frac{\partial \Phi}{\partial z}(\hat{\mathbf{n}}, z) \quad (1)$$

where Φ is the Newtonian gravitational potential at redshift z , $\hat{\mathbf{n}}$ is a unit vector along a line of sight, $T_0 = 2.725 \text{ K}$ is the CMB temperature at present time and $z_{\text{LS}} \approx 1089$ is the redshift at the surface of last scattering.

The gravitational potential, Φ , is related to the matter density fluctuation via Poisson's equation (Eq. 7.14, Peebles 1980);

$$\nabla^2 \Phi(\hat{\mathbf{n}}, z) = 4\pi G a^2 \rho_m(z) \delta(\hat{\mathbf{n}}, z) \quad (2)$$

where a is the scale factor normalised to unity at redshift zero. By recalling that $\rho_{\text{crit}}(0) = 3H_0^2/8\pi G$ and $\Omega_m = \rho_m(0)/\rho_{\text{crit}}(0)$, the Fourier transform of the gravitational potential is

$$\Phi(\mathbf{k}, z) = -\frac{3}{2}\Omega_m \left(\frac{H_0}{k}\right)^2 \frac{\delta(\mathbf{k}, z)}{a}. \quad (3)$$

Unfortunately, the ISW contribution to the CMB primary anisotropy is less than 10 per cent for $l \gtrsim 10$ and to make matters worse, the total anisotropy signal is dominated by cosmic variance at smaller l (i.e. larger angle) where most of the ISW signal is expected to be (e.g. Hu & Scranton 2004). To isolate the ISW signal one must cross-correlate the temperature fluctuation with a tracer of gravitational potential projected on the sky (Crittenden & Turok 1996). For this purpose, one can use the simple 2-point statistics to compute the angular cross-correlation of the temperature and galaxy fluctuation maps in real space,

$$w_{gT}(\theta) = \langle \delta_g(\hat{\mathbf{n}}_1) \Delta_T(\hat{\mathbf{n}}_2) \rangle \quad (4)$$

where $\hat{\mathbf{n}}_1 \cdot \hat{\mathbf{n}}_2 = \cos\theta$. To calculate the theoretical expectation for the real space cross-correlation, we start by computing the angular cross-power spectrum of the galaxy overdensity and ISW temperature perturbation fields;

$$C_{gT}^{\text{ISW}}(l) \equiv \langle \delta_{g,lm} \Delta_{T,l'm'}^* \rangle. \quad (5)$$

Firstly, we need to expand the galaxy density fields, $\delta_g(\hat{\mathbf{n}}, z)$, in spherical harmonics and Fourier transform them. For a galaxy survey with a selection function $\phi_g(z)$ and linear bias $b_g(z)$, this is

$$\delta_{g,lm} = i^l \int \frac{d^3k}{(2\pi)^3} \int dz 4\pi j_l(k\chi) Y_{lm}^*(\hat{\mathbf{k}}) \times b_g(z) \phi_g(z) \delta(\mathbf{k}, z) \quad (6)$$

where $j_l(y)$ is the spherical Bessel function of the first kind of rank l , $Y_{lm}(\hat{\mathbf{k}})$ is the spherical harmonic function and χ is a comoving distance which is an implicit function of z through the relation $d\chi = c/H(z) dz$. In obtaining Eq. 6, we use the orthonormality of Y_{lm} in their expansion of a plane wave (e.g. Scharf et al. 1992);

$$\exp(-i\mathbf{k} \cdot \hat{\mathbf{n}}\chi) = 4\pi \sum_{lm} i^l j_l(k\chi) Y_{lm}(\hat{\mathbf{n}}) Y_{lm}^*(\hat{\mathbf{k}}) \quad (7)$$

Similarly, for the ISW temperature fluctuation, by putting together Eq. 1, 3 and 7, this is

$$\Delta_{T,lm}^{\text{ISW}} = i^l \int \frac{d^3k}{(2\pi)^3} \int dz 4\pi j_l(k\chi(z)) Y_{lm}^*(\hat{\mathbf{k}}) \times 3\Omega_m T_0 \left(\frac{H_0}{kc}\right)^2 \frac{\partial}{\partial z} \left[\frac{\delta(\mathbf{k}, z)}{a(z)} \right] \quad (8)$$

For a flat-sky approximation (Limber 1953), following Afshordi et al. (2004) and realising that in linear perturbation theory $\delta(\mathbf{k}, z) = D(z) \delta(\mathbf{k}, 0)$ and

$$\langle \delta(\mathbf{k}_1) \delta(\mathbf{k}_2) \rangle = (2\pi)^3 \delta_{\text{Dirac}}(\mathbf{k}_1 - \mathbf{k}_2) P(k), \quad (9)$$

from Eq. 5, 6 and 8, $C_{gT}^{\text{ISW}}(l)$ can be simplified to

$$C_{gT}^{\text{ISW}}(l) = \frac{4}{(2l+1)^2} \int dz P(k) W_{\text{ISW}}(z) W_g(z). \quad (10)$$

$W_{\text{ISW}}(z)$ and $W_g(z)$ are the ISW and galaxy window functions defined as

$$W_{\text{ISW}}(z) \equiv 3\Omega_m T_0 \left(\frac{H_0}{c}\right)^2 \frac{d}{dz} \left[\frac{D(z)}{a(z)} \right] \quad (11)$$

and

$$W_g(z) \equiv b_g(z) \phi_g(z) D(z) \quad (12)$$

where $k \approx (l+1/2)/\chi(z)$, $D(z)$ is the linear growth factor given by the fitting formula of Carroll et al. (1992) and $P(k)$ is the linear power spectrum at redshift zero. The survey selection function is given by

$$\phi_g(z) \equiv \frac{\chi^2 n_c(\chi)}{\int d\chi \chi^2 n_c(\chi)} = n(z) \frac{H(z)}{c} \quad (13)$$

where $n_c(\chi)$ is the comoving number density and $n(z)$ is the normalised redshift distribution, $N(z)$, of the galaxies in the survey. Finally, $w_{gT}^{\text{ISW}}(\theta)$ is related to the cross-power spectrum via the expansion in Legendre polynomials;

$$w_{gT}^{\text{ISW}}(\theta) = \sum_{l=2}^{\infty} \frac{2l+1}{4\pi} P_l(\cos\theta) C_{gT}^{\text{ISW}}(l). \quad (14)$$

We set the monopole ($l=0$) and dipole ($l=1$) contribution to zero, as it is done in the *WMAP* maps (§2.1). The contributions of the monopole and dipole are significant and overpredict w_{gT}^{ISW} by ≈ 10 per cent (Cabr e et al. 2006). The summation in Eq. 14 converges earlier than $l \approx 500$ but we set our upper limit to $l = 1000$ which provides sufficiently stable models without sacrificing too much computing time. The linear power spectrum is computed using

$$P(k) = A k^{n_s} T^2(k) \quad (15)$$

where n_s is the scalar spectral index and A is the normalisation factor with the value set by σ_8 . We use the transfer function, $T(k)$, fitting formula of Eisenstein & Hu (1998). Our fiducial models assume a Λ CDM Universe with $\Omega_\Lambda = 0.73$, $\Omega_m = 0.27$, $f_{\text{baryon}} = 0.167$, $\sigma_8 = 0.8$, $h = 0.7$ and $n_s = 0.95$. Note that, for a flat Universe with $\Omega_m = 1$, the linear growth factor is equal to the scale factor, a , at all redshifts and $W_{\text{ISW}}(z)$ vanishes, hence in this case we expect no correlation between large-scale-structure and the CMB.

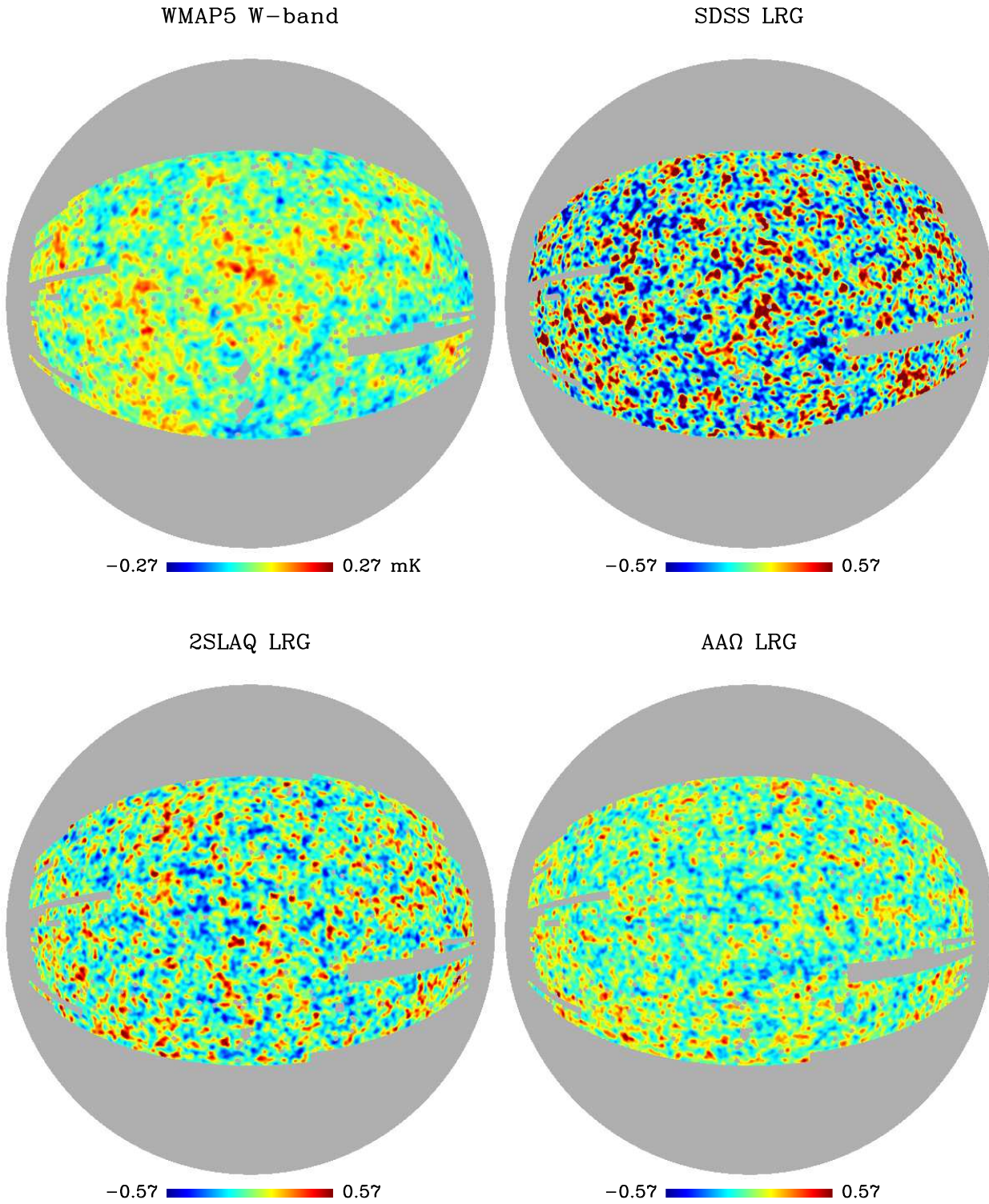


Figure 2. The 1° smoothed map of W-band data and galaxy number overdensity for SDSS, 2SLAQ and AAΩ LRG (Ubercal) after applying KQ75 and SDSS-DR5 mask.

4 CROSS-CORRELATION TECHNIQUE

Firstly, each galaxy sample is pixelised into equal area pixels on the sphere using the HEALPix (Górski et al. 2005) format, following the standard resolution and ordering scheme of the publicly-available *WMAP5* temperature map (i.e. nested, res=9). The most conservative temperature mask, extended temperature analysis (KQ75), plus point source catalogue mask are then applied to the temperature maps (§2.1) and the pixelised galaxy distributions, discarding approximately 30 per cent of the entire sky. Additionally, in order to estimate fairly the galaxy background density and a robust cross-correlation result, the DR5 coverage mask including quality holes are applied to the data. We only restrict the data to the most contiguous region of the NGC and therefore exclude the SDSS stripes 39, 42 and 43 in the DR5 coverage mask. After applying ‘KQ75 \cup point source \cup DR5’ mask, 516,507 out of 3,145,728 pixels (all sky) are admitted for the cross-correlation analysis.

The galaxy number overdensity, $\delta_g(\hat{\mathbf{n}})$, is then calculated from the galaxy distribution maps and assigned to each pixel;

$$\delta_g(\hat{\mathbf{n}}) = \frac{n_g(\hat{\mathbf{n}}) - \bar{n}_g}{\bar{n}_g} \quad (16)$$

where n_g and \bar{n}_g are the number of galaxies and its average for the sample of interest. Fig. 2 shows the W-band temperature fluctuation map and δ_g map for SDSS, 2SLAQ and AA Ω LRG, smoothed with Gaussian beam of 1° Full Width at Half Maximum (FWHM).

The two-point cross-correlation function at angular separation θ is computed using

$$w_{gT}(\theta) = \frac{\sum_{ij} f_i \delta_g(\hat{\mathbf{n}}_i) f_j \Delta_T(\hat{\mathbf{n}}_j)}{\sum_{ij} f_i f_j} \quad (17)$$

where f_i is the fraction of pixel i within the unmasked region, $\hat{\mathbf{n}}_i \cdot \hat{\mathbf{n}}_j = \cos \theta$ and Δ_T is the CMB temperature anisotropy measured by *WMAP5* with the monopole and dipole contribution subtracted off. However, as we use relatively fine resolution pixels and weighting by the unmasked fraction does not alter our measurement, Eq. 17 is simply $w_{gT}(\theta) = \langle \delta_g(\hat{\mathbf{n}}_1) \Delta_T(\hat{\mathbf{n}}_2) \rangle$.

It is a well known fact that bins in the correlation function are correlated because the same points (or pixels in this case) can appear in many different pairs which are included in different bins, especially at large scales. To correctly estimate the statistical significance of the results, one needs to consider the full covariance matrix, \mathbf{C}_{ij} . Here, we construct the full covariance matrices using the *jackknife* re-sampling. In order to obtain a sufficiently stable covariance matrix, the jackknife subsamples of approximately twice the number of angular bins being considered are needed. For the number of angular bins considered in this study, we split the masked temperature/overdensity map into 24 subfields with approximately equal area. The 24 jackknife subsamples are constructed from these fields, each one leaving out a different subfield. The $w_{gT}(\theta)$ are computed for each jackknife subsample and the covariance matrix is

$$\mathbf{C}_{ij} = \frac{N_J - 1}{N_J} \sum_{m=1}^{N_J} [(w_{gT,m}(\theta_i) - \overline{w_{gT}}(\theta_i))$$

$$\times (w_{gT,m}(\theta_j) - \overline{w_{gT}}(\theta_j))] \quad (18)$$

where $N_J = 24$ in this case, $w_{gT,m}(\theta_i)$ and $\overline{w_{gT}}(\theta_i)$ are the cross-correlation measured from the m th jackknife subsample and the average of all the subsamples in the i th bin, respectively. Note that the difference between $\overline{w_{gT}}(\theta)$ and $w_{gT}(\theta)$ estimated using the whole sample is negligible. The reason for multiplying $N_J - 1$ is because the jackknife subsamples are not independent. The statistical uncertainty for each individual angular bin is contained in the diagonal elements of the covariance matrix.

5 RESULTS AND ANALYSIS

5.1 LRG–*WMAP5*

The cross-correlation results of the LRG distributions with the *WMAP5* temperature maps using the three highest-frequency data plus the ILC are shown in Fig. 3. The errors are 1σ statistical errors estimated from jackknife re-sampling of 24 subfields as described in §4. Generally, the results using different *WMAP* bands are in good agreement (within the 1σ error) for all three LRG samples. The achromatic results indicate that the contamination from effects such as dust, synchrotron and free-free emission which are frequency-dependent in nature are minimal or at least subdominant compared to our statistical uncertainties. This also applies to a lesser extent to the thermal Sunyaev–Zeldovich (Sunyaev & Zeldovich 1980) effect, although for the bands shown, the difference in the SZ and CMB spectral slopes is only ≈ 30 per cent. However, we shall see in §7 that there is still a strong suggestion that other systematic effects may still be contaminating the SDSS and 2SLAQ results.

We first consider our new and higher redshift sample of 800 000 AA Ω LRGs. This sample shows virtually no positive correlation with the CMB data. If anything, the data show a slight anticorrelation out to large scales, possibly to $\theta \lesssim 1^\circ$ ($\approx 30h^{-1}$ Mpc at the median redshift of the sample), although the signal to noise is still low. This weak anticorrelation is observed in all *WMAP5* frequency bands under study here (the most right column of Fig. 3) with the exception of the Q band which only shows zero correlation at best with a possible zeropoint shift towards very large scales. As for the SDSS and 2SLAQ results the cross-correlation with the ILC map gives a systematically lower amplitude (more negative in AA Ω case) than other bands. Given the relatively large scales of the null result in the AA Ω –*WMAP5* CCF and the amplitude of the expected ISW signal (see Fig. 4), it would seem extremely unlikely that the positive correlation of the ISW effect could be cancelled out by the negative contribution from the thermal SZ effect. If this result is real and not due to some systematic effects, the implications for the view that the Universal expansion is accelerating, could be profound.

In the case of the SDSS and 2SLAQ LRG samples, our results are similar to those of the previous authors who have analysed similar datasets. We observe marginally significant positive correlations in the Q , V and W bands where the measured $w_{gT}(\theta)$ ’s are similar in terms of their amplitudes and angular extents for each sample although the signal is weaker in the SDSS sample. The ILC results are slightly

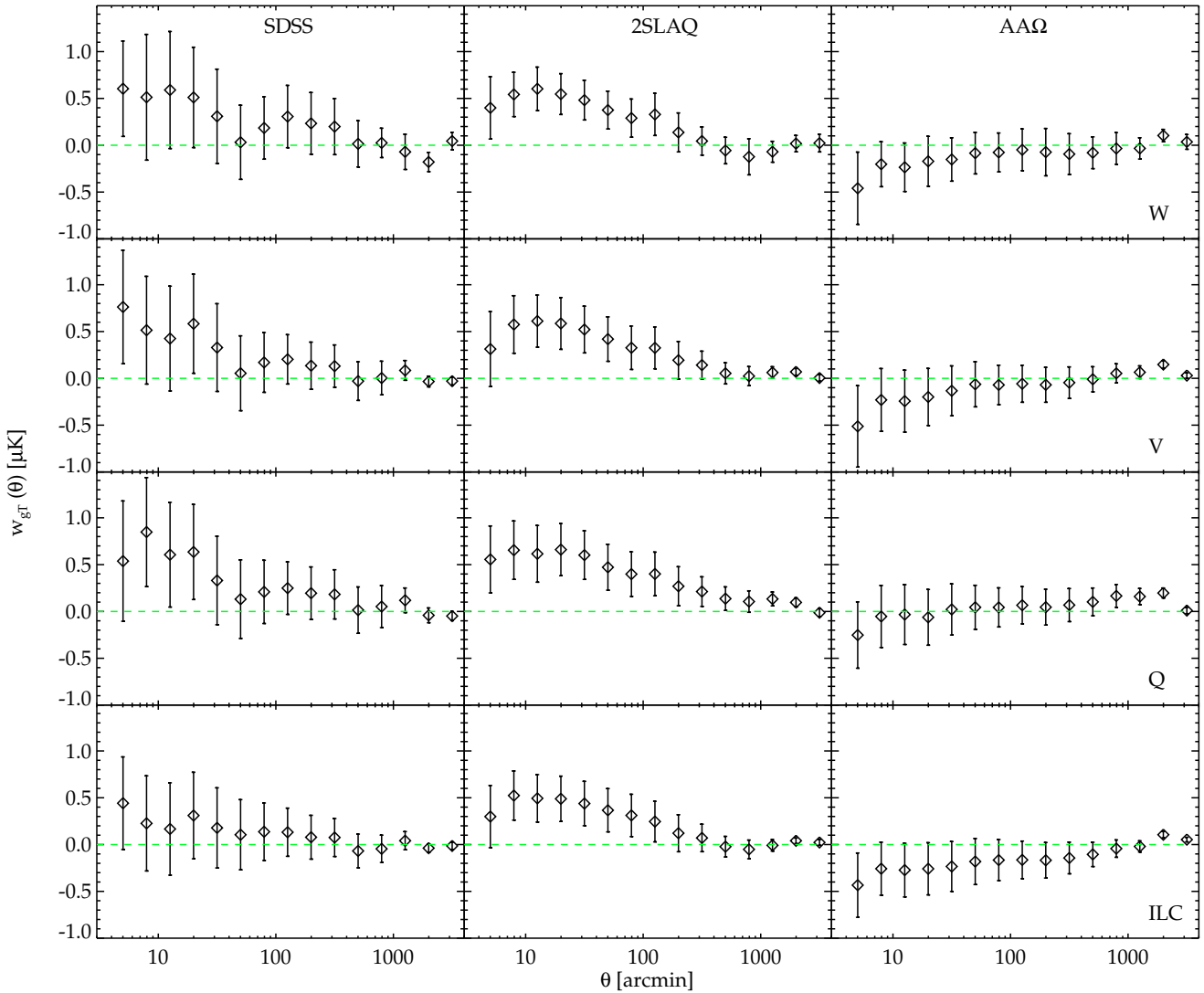


Figure 3. The cross-correlation results of *WMAP5* *W*, *V* and *Q* band including the ILC map (top to bottom) with the SDSS, 2SLAQ and AAΩ LRG (left to right).

lower than the other bands in both samples but otherwise still within 1σ error. Our SDSS results can be compared to the lowest redshift-bin sample of Scranton et al. (2003) who used the LRGs extracted from the SDSS DR2 following Eisenstein et al. (2001) but with a much fainter magnitude limit, $i < 21$, and divided their samples into redshift slices using photo- z . The results are similar in terms of amplitude but our errors are slightly smaller due to our larger area coverage ($\approx 7600 \text{ deg}^2$ as opposed to $\approx 3400 \text{ deg}^2$) although their object numbers are ≈ 7 times higher than ours owing to the broader $N(z)$ and fainter flux cut. The 2SLAQ results are comparable to the ‘SDSS LRG’ results of Giannantonio et al. (2008). These authors used the MegaZ-LRG photo- z catalogue of Collister et al. (2007), covering the redshift range 0.4–0.7 with a colour-magnitude selection similar to our 2SLAQ sample but a slightly fainter flux limit, $i_{\text{dev}} < 20$ as opposed to 19.8. In the LRG panel of their Fig. 4, we see that their result has similar amplitude

and errors (jackknife) to our 2SLAQ result. Although their Monte Carlo methods give somewhat larger errors than the jackknife estimations, the statistical significance estimated using errors drawn from both methods are very similar, 2.2–2.5 σ for their LRG catalogue. Padmanabhan et al. (2005) has also performed the analysis with a similar LRG sample but using the angular cross-power spectrum, C_l , making a direct comparison to our results difficult. The sample these authors used is somewhat similar to the Eisenstein et al. (2001) selection but with the flux cut as faint as 2SLAQ in ‘CutII’, resulting in a redshift distribution similar to our SDSS and 2SLAQ LRG samples combined, although they limited the redshift of the sample to $0.2 < z < 0.6$ using their template-fitting photo- z . The positive correlation is detected at 2.5 σ , similar to Giannantonio et al. (2008) although the sample they used only covers half as much sky. We conclude that our analyses are broadly reproducing pre-

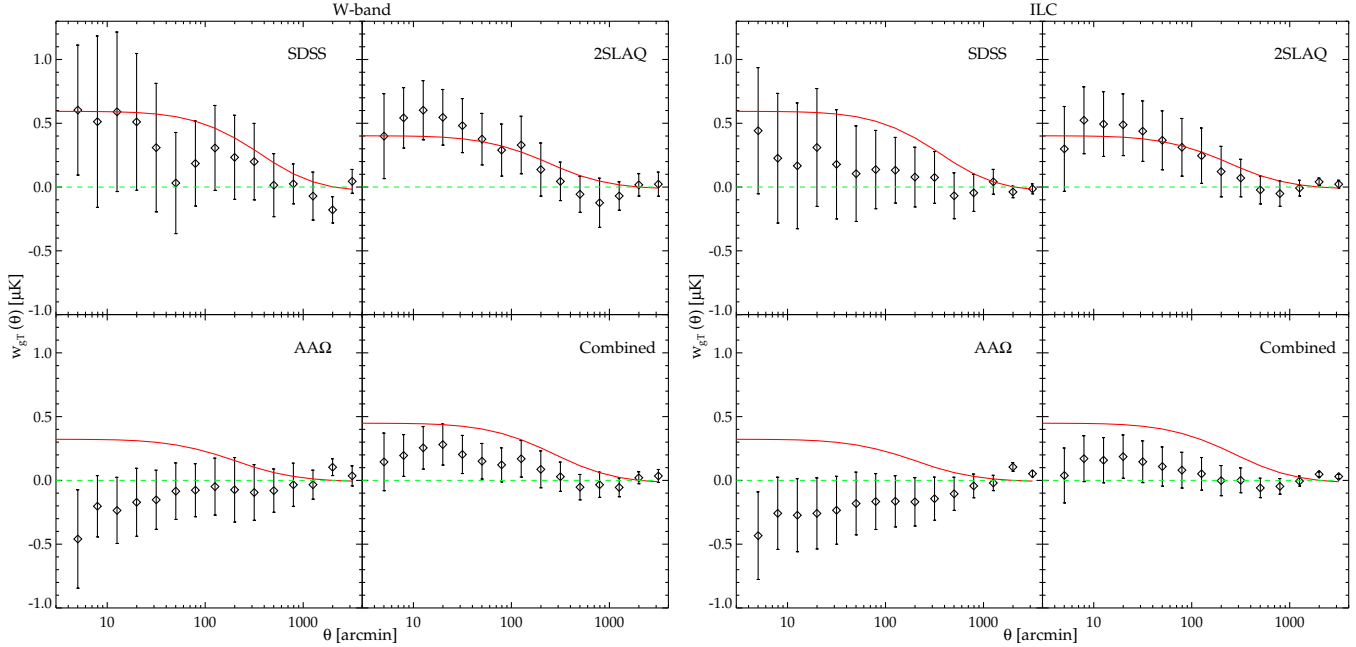


Figure 4. The LRG–*WMAP5* cross-correlation results using *W*-band and ILC map compared to the theoretical predictions (red solid lines), assuming the standard Λ CDM and the galaxy linear bias (b_g) of 2.10, 1.99, 2.2 and 2.1 for SDSS, 2SLAQ, AA Ω -LRG and the combined sample respectively. The stellar contamination correction for each sample has been applied to the corresponding model. In the ‘Combined’ panels, the cross-correlation results of the quadrature-error weighted mean of the three LRG samples are compared to the average model predictions.

vious results in these $0.25 < z < 0.6$ LRG redshift ranges, both in terms of their amplitude and statistical significance.

5.2 Comparison to Models

Fig. 4 shows the comparison of our results to the theoretical expectation as described in §3. The galaxy selection functions used in construction of these models are given by the normalised $N(z)$ of the sample as shown in Fig. 1 (see also §2.2). The galaxy bias in the model is estimated from the angular autocorrelation function, $w_g(\theta, \bar{z})$, of each LRG sample relative to the underlying dark matter clustering, $b_g^2(\bar{z}) = \xi_g(r, \bar{z})/\xi_m(r, \bar{z})$, where we assume the linear scale-independent bias and measure its value at large scales ($\approx 10 h^{-1}$ Mpc). The matter $\xi(r, \bar{z})$ is estimated for the same fiducial cosmology as described in §3 and then projected onto the sky using the corresponding $n_g(z)$. This gives an unbiased prediction which can be compared to the measured $w_g(\theta, \bar{z})$ and allows $b_g(\bar{z})$ to be extracted from their relative amplitudes (see Sawangwit et al. in prep for the full detailed analyses). Note that, we assume non-evolving bias and denote the bias estimated from each sample as the bias at the corresponding average redshift which is reasonable, given the narrow redshift ranges of our samples. The galaxy bias measured in this way can also be viewed as an effective value for each sample. The models shown in Fig. 4 use $b_g(\bar{z})$ of 2.10 ± 0.04 , 1.99 ± 0.02 and 2.20 ± 0.02 for the SDSS, 2SLAQ and AA Ω samples, respectively. These values are taken from Sawangwit et al. (in prep) and are compatible with the values measured by other authors, e.g. Tegmark et al. (2006), Padmanabhan et al. (2007) whose $b_g(0.35) = 1.9 \pm 0.07$ and $b_g(0.55) = 1.85 \pm 0.05$ as compared to our SDSS and 2SLAQ

LRG, respectively. The b_g value of Tegmark et al. (2006) was measured from a sample of $z \approx 0.35$ LRGs similar to what we call SDSS LRG sample here but without the bright limit cut (see §2.2.1) hence allows under-luminous objects and main galaxies into their sample. And as a result we expect their bias to be somewhat lower than ours.

As emphasised earlier, the AA Ω LRG sample shows no positive correlation with the *WMAP5* data and perhaps even a slight negative correlation. We then combined the *W*-band data between $12'–120'$, and found the amplitude of the CCF and its jackknife error (1σ) is $-0.07 \pm 0.2 \mu\text{K}$. This is consistent with the null hypothesis (only $\approx 0.4\sigma$ deviation) and rejects the ISW signal expected in the standard models at $\approx 1.9\sigma$ or at 5% significance after the stellar contamination has been taken into account in the predicted signal (see §6.3). Performing a similar statistical analysis on the cross-correlation results using the ILC map gives a slightly higher significance of rejecting the standard model ISW hypothesis (2.2 σ , see Table 2).

Additionally, to test that the zero correlation in the AA Ω results is not due to its faint limit making the sample incomplete, we have cut the faint limit of the sample back in steps of 0.25 mag to 20.0 (see §6.2 and Sawangwit et al. 2009). The amplitude of the CCF between $12'–120'$ for $i < 20.25$ (denoted by AA Ω^* in Table 2) is -0.1 ± 0.2 for *W*-band data and -0.2 ± 0.21 for the ILC map. The ISW model prediction is then re-computed taking into account the corresponding $n(z)$ and linear bias, including the correction for stellar contamination at the same level as the main AA Ω sample. The significance of rejection of the standard model for the $i < 20.25$ AA Ω sample is slightly higher than that

Table 2. The significance tests of the cross-correlation results using the *WMAP* *W*-band data and ILC maps. The measurements are tested against the expected ISW prediction in the standard Λ CDM model and null result hypothesis. Column 5 gives the amplitudes and 1σ jackknife errors of the data binning between $12' - 120'$. Column 6 gives the significance of the deviation of the value in column 5 relative to ISW/null signal hypothesis.

Sample	\bar{z}	Number	$b_g(\bar{z})$	$w_{gT}(12' - 120')$ μK	Deviation significance (ISW,null)	
<i>W</i> -band:	SDSS	0.35	106,699	2.10 ± 0.04	0.25 ± 0.33	$(1.0\sigma, 0.8\sigma)$
	2SLAQ	0.55	655,775	1.99 ± 0.02	0.34 ± 0.21	$(0.2\sigma, 1.6\sigma)$
	AA Ω	0.68	800,346	2.20 ± 0.02	-0.07 ± 0.20	$(1.9\sigma, 0.4\sigma)$
	AA Ω^*	0.67	375,056	2.37 ± 0.03	-0.10 ± 0.20	$(2.2\sigma, 0.5\sigma)$
	Combined	0.60	1,562,820	2.10 ± 0.01	0.15 ± 0.17	$(1.0\sigma, 0.9\sigma)$
	Weighted mean	–	–	–	0.14 ± 0.14	$(1.3\sigma, 1.0\sigma)$
ILC map:	SDSS	0.35	106,699	2.10 ± 0.04	0.19 ± 0.33	$(1.2\sigma, 0.6\sigma)$
	2SLAQ	0.55	655,775	1.99 ± 0.02	0.27 ± 0.22	$(0.5\sigma, 1.2\sigma)$
	AA Ω	0.68	800,346	2.20 ± 0.02	-0.18 ± 0.22	$(2.2\sigma, 0.8\sigma)$
	AA Ω^*	0.67	375,056	2.37 ± 0.03	-0.20 ± 0.21	$(2.5\sigma, 1.0\sigma)$
	Combined	0.60	1,562,820	2.10 ± 0.01	0.07 ± 0.17	$(1.4\sigma, 0.4\sigma)$
	Weighted mean	–	–	–	0.07 ± 0.13	$(2.0\sigma, 0.5\sigma)$

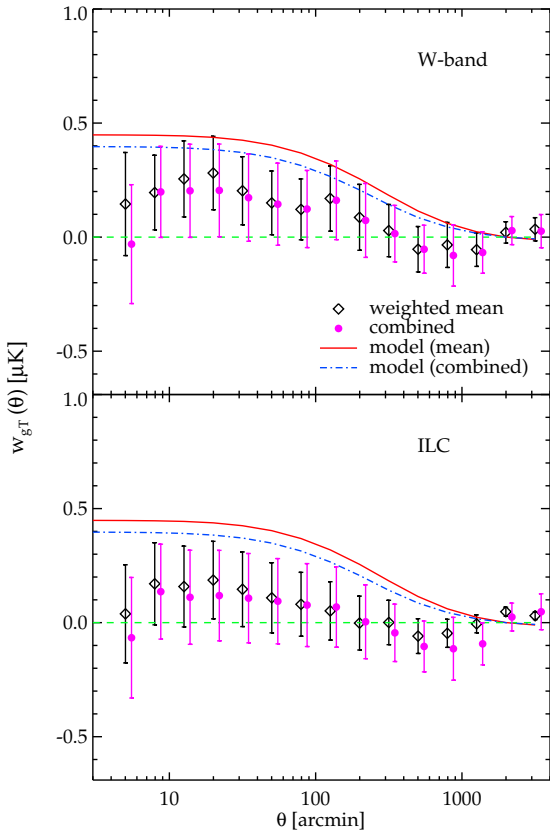


Figure 5. *Top:* The *W*-band cross-correlation results of the combined sample (solid circles) compared to the quadrature-error weighted mean of the three LRG sample (diamonds). Also shown are the standard model predictions by taking a weighted mean (solid line) of the models of three LRG samples and for the combined sample (dot-dash line). *Bottom:* Same as above but for the ILC map rather than *W*-band data

of the main AA Ω sample, at 2.2σ and 2.5σ for *W*-band and ILC map, respectively.

The measured w_{gT} for the SDSS LRG agrees reasonably well with the theoretical expectation at angles $\lesssim 30'$ although not at high statistical significance. However, the same cannot be said for the angle beyond this scale and up to $\approx 600'$ where the cross-correlation appears to be less than the expected signal although still not at high significance. One may be inclined to conjecture that this could be due to the negative contribution coming from the thermal SZ effect, but at this redshift $100'$ corresponds to $\approx 20 h^{-1}\text{Mpc}$ which would be too large a scale to be caused by hot gas in galaxy clusters. Although the clusters do cluster among themselves, the contribution to any extend SZ effect is likely to be small (Myers et al. 2004). Besides, there is no physical reason why should SZ effect only affect the highest redshift sample. The most likely explanation for this appears to be a statistical fluctuation which means that our SDSS LRG measurement rejects neither the ISW expectation nor the zero correlation at more than $\approx 1\sigma$ significance level. If we bin the data in the angular range $12' - 120'$ into a single bin, the correlation amplitude and its jackknife error (1σ) is $0.25 \pm 0.33 \mu\text{K}$ which deviates from the null result hypothesis by only 0.8σ and from the standard model by 1.0σ . For the 2SLAQ case, as in other studies, the positive cross-correlation signal agrees very well with the expected ISW signal in the standard cosmology in terms of its amplitude and angular extent. Nevertheless, the 2SLAQ sample's rejection of the null result is still only at the 1.2 - 1.6σ significance level (see Table 2).

5.3 The Combined LRG sample

We shall now consider the cross-correlation of the combined LRG sample with the CMB data. In our first method of combining the three LRG samples we shall treat these as three independent surveys and then test this assumption by presenting the cross-correlation result for the combined 1.5 million LRG sample, complete with its own direct jackknife error analysis, to check that they agree.

First, the three CCF's of the SDSS, 2SLAQ and AA Ω samples are combined by weighting inversely in quadrature according to the statistical errors of each sample (see bottom right panels of Fig. 4 and also Fig. 5). The model (red solid line in Fig. 4) is estimated by taking an average of the ISW models of the three LRG samples. We find that the rejection significance is 1.3σ for the standard ISW model and 1.0σ for the null result in the W band. In the ILC band the significance of the rejection of the ISW model rises to 2.0σ and the significance of rejection of the null result reduces to 0.5σ . Table 2 gives the summary of all the significance tests performed. We conclude that while the ISW standard model is still consistent with the CCF result from the three combined, weighted LRG samples it is now more consistent with the null result due to the inclusion of the AA Ω data.

Second, for comparison, we also present the results of cross-correlating the combined LRG sample with the WMAP5 data i.e. we now treat the combined sample of ≈ 1.5 million LRGs as a single sample for cross-correlating with, in turn, the WMAP5 W and ILC CMB data. A full jackknife error analysis was carried out in the same way as for the individual samples. We expect the results to be similar to the weighted combination of the three samples' CCF's as presented above. Fig. 5 shows the comparison between these results. The models for the combined samples are computed following the procedure described in §3 assuming the linear galaxy bias (given in Table 2) estimated from the angular autocorrelation function and $N(z)$ of 1.5 million LRGs. Table 2 again shows the significances of rejection of the standard model and the null results. We see that the observational results in both cases are very similar. For both bands, the significances are given in Table 2. The results are again very similar to those where the weighted mean was adopted. The cross-correlation results are again as consistent with the zero correlation as they are with the standard ISW model for the W band. The ILC band again more significantly rejects the ISW model than the null result.

Clearly the preference for the null result over the standard model prediction depends on the accuracy of the new AA Ω result. We test the robustness of the AA Ω result in §6.

5.4 χ^2 fits

For completeness, we also quantified the goodness-of-fit of our measurements to the expected ISW signal or null result hypothesis by calculating the *chi-square*, χ^2 , which uses the normal size bin as shown in Fig. 4 and takes into account the possible correlation of the bins through the use of the covariance matrix (§4). The χ^2 is given by

$$\chi^2 = \sum_{i,j} \mathbf{C}_{ij}^{-1} [w_{gT}(\theta_i) - w_{gT}^{\text{ISW}}(\theta_i)] \cdot [w_{gT}(\theta_j) - w_{gT}^{\text{ISW}}(\theta_j)] \quad (19)$$

where \mathbf{C}_{ij}^{-1} is the inverse of covariance matrix, $w_{gT}(\theta_i)$ is the measured angular cross-correlation and w_{gT}^{ISW} is the theoretical expectation assuming the standard Λ CDM cosmology (see Fig. 4) which can be replaced by zero when testing the zero correlation hypothesis. Using the galaxy linear bias, b_g , and $N(z)$ for each sample as mentioned in §5.2, the χ^2 tests were performed for the angular bins between $12'$ – $120'$, inclusively. The lower limit is set approximately to the best WMAP5 resolution in the W band ($\approx 12'$).

The significances obtained from the χ^2 method generally confirmed the results using the $12'$ – $120'$ bin, especially those of the main LRG samples. For example, assuming standard model parameters, the SDSS- W band results give $\chi^2=19.4$ for the predicted ISW signal and 17.7 for the zero correlation hypothesis. For the 2SLAQ results, using the standard model gives $\chi^2 = 13.2$ and relative to the null result gives $\chi^2 = 11.5$. These χ^2 were computed for 6 degrees-of-freedom (d.o.f). Using the χ^2 distribution, the SDSS results deviate from the ISW model and null result at 4 and 7 per cent statistical significance, respectively. The 2SLAQ results agree with the ISW model with the reduced chi-square, $\chi^2/\text{d.o.f.}$, of order of unity and reject the zero correlation hypothesis at 1.5σ significance. The AA Ω results gave $\chi^2 = 11.7$ and $\chi^2 = 4.4$ for the ISW model and null correlation respectively, corresponding to the chances of agreement of 7% and 62%. These all agree reasonably well with the large-bin significances presented in Table 2. However, the similar χ^2 significance tests of the combined sample and some ILC individual samples did not perform very consistently, occasionally giving pathological results and poor agreement with the $12'$ – $120'$ bin and this is why we have only quoted the simpler, single large-bin significances in Table 2.

6 ROBUSTNESS TESTS

Given that the AA Ω LRGs comprise a new sample, there is no previous measurement that can be directly compared to our own. We now present the result of tests we have done in order to check the robustness of our new result.

6.1 Random realisations and simulated CMB Maps

Here we generate 100 random realisations for each of the sample. Each realisation has the same number density as the sample it tries to mimic. Note that these random realisations are unclustered. The results are shown in Fig. 6. The jack-knife errors that we use are seen to be much larger than the standard deviation of the random catalogues (inner green shaded region). This is expected because the random catalogues are unclustered unlike the LRGs. The means of these random realisations are consistent with zero and show no sign of bias except perhaps at the smallest scales of the SDSS sample.

We have also made simulated CMB temperature anisotropy maps and cross-correlated these with the three LRG samples. A simulated CMB map is generated as a realisation of random gaussian fields on a sphere with the fluctuation characterised by WMAP5 best-fit power spectrum. The simulated maps are also convolved with a Gaussian beam with FWHM similar to the WMAP W -band, i.e. $12'.6$. The cross-correlation results are shown in Fig. 6. The standard deviation of 100 CMB random realisations (outer grey shaded region) are roughly consistent with our jack-knife estimates especially at small and intermediate scales but somewhat larger at large scales.

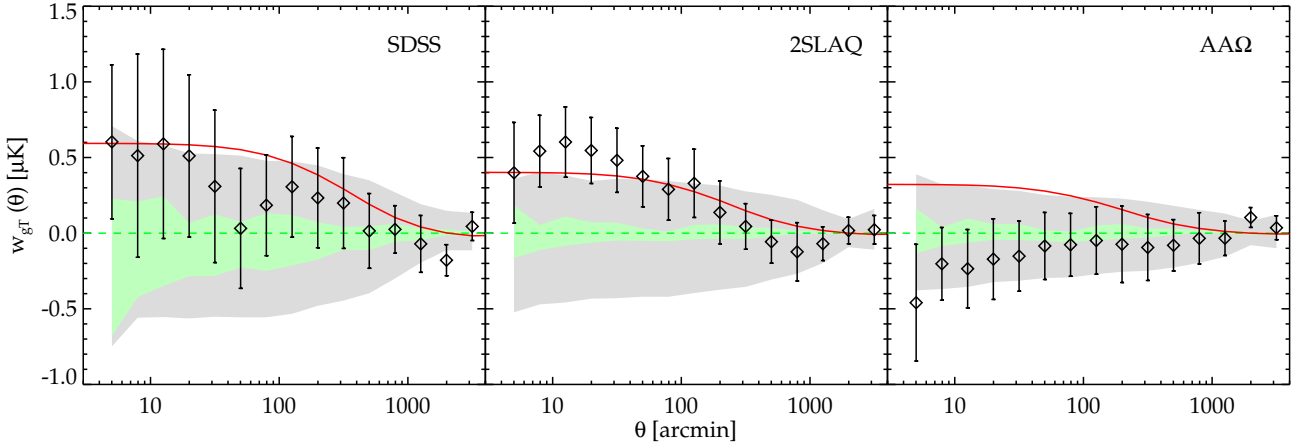


Figure 6. The cross-correlation results (diamonds) of three LRG samples and their jackknife errors (1σ) compared to the results of using 100 random realisations of each LRG sample (inner green shaded region) and 100 simulated CMB maps (outer grey shaded region). The shaded area signify a standard deviation in the measurement of 100 realisation for each case. Note that the means of these random realisations are consistent with zero as can be seen from their symmetry about the zero line. The solid line is again the theoretical prediction of the ISW signal in standard Λ CDM.

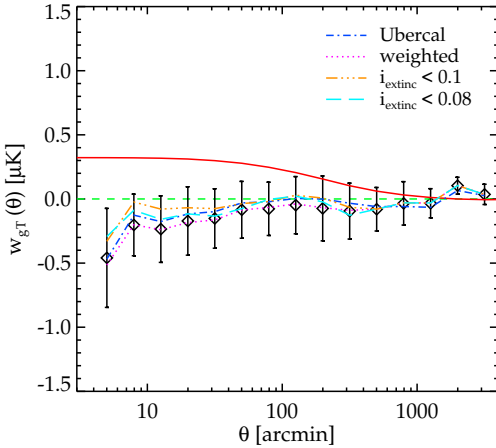


Figure 7. The cross-correlation of the AA Ω LRG to W-band data using the original SDSS photometry (diamond) compared to the measurements using ‘ubercalibration’ (dot-dash line), the stripe weighted (dotted line) and when the data is restricted to the region where galactic extinction in i -band less than 0.1 (dot-dot-dash line) and 0.08 (long dashed line) magnitude.

6.2 Photometry test

Next, we look to see if the AA Ω cross-correlation measurement is robust by comparing the result from the SDSS ‘ubercalibration’ of Padmanabhan et al. (2008) with that from the standard SDSS calibration. Fig. 7 shows that the results are stable to whichever calibration we used. We further looked for systematic effects in the original photometry by weighting SDSS stripes according to their overall number density. The physical motivation for this arises from the SDSS observing strategy and the fact that a slightly different calibration for different nights could affect the source density as a function of the SDSS stripe, given our faint limit. We observe a hint of these variations although not at

a high level and use these to correct the source densities in each stripe as mentioned. However, such variations seems to be weaker when using the ubercalibration as opposed to the standard one. The result of weighting according to the stripe number density is shown in Fig. 7 and again the result appears robust when this filter is applied to the original data.

Although we work at a relatively high galactic latitude, it is possible that in some regions of the sky, high galactic dust obscuration could result in lower detections of faint objects. Furthermore, that same dust obscuration patch could be a source of contamination in the CMB data in the sense that the temperature in that particular region could be systematically raised by the dust emission and hence results in a false anticorrelation. To test this, we exclude the region where the extinction is greater than 0.1 mag in the i -band which discards ≈ 15 percent of the data. We observe no difference to our main results, even when a more aggressive limit, $i_{\text{extinction}} < 0.08$ (23 per cent discard), is applied (see Fig. 7). Note that when similar tests are performed using extinction in the SDSS r -band instead, we again obtain results which are consistent with those presented in §5 for all three LRG samples.

We then cut back the i -band limit of the AA Ω sample in 0.25 mag steps from $i = 20.5$ to $i = 20.0$ while keeping the other conditions the same. These results are compared with the result at $i < 20.5$ in Fig. 8. Again the results appear robust. We have also made tests of the single epoch SDSS photometry using deeper Stripe 82 (Abazajian et al. 2009) and the William Herschel Deep Field (WHDF, Metcalfe et al. 2001) data. Both these comparisons showed that the SDSS photometry in r , i and z bands showed good agreement with the deeper data until the errors showed a significant increase beyond the limits $r = 22.0$, $i = 21.0$ and $z = 20.2$.

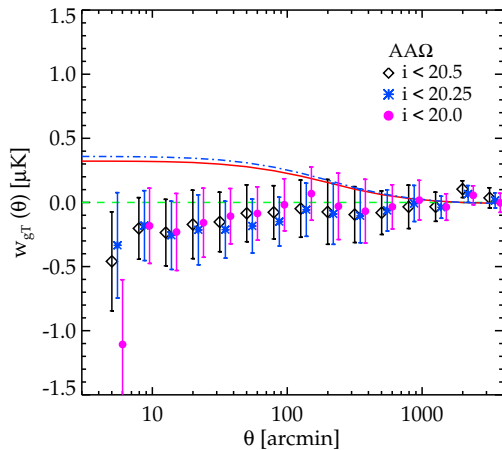


Figure 8. The cross-correlation of the AAΩ LRG to W-band data compared to the measurements using the same colour–colour selection sample but with brighter faint–limit cut, $i_{\text{deV}} < 20.25$ and $i_{\text{deV}} < 20.0$. Only the theoretical expectation of the full (solid line) and $i_{\text{deV}} < 20.25$ (dash-dot line) sample are shown. The data points are shifted slightly for displaying purposes.

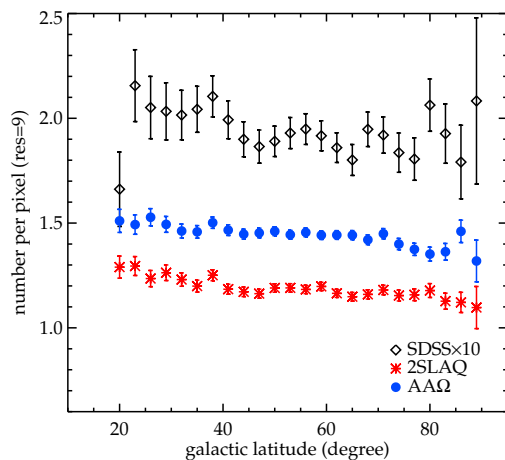


Figure 9. The object numbers per pixel as a function of galactic latitude, b . Recall that we use equal area ($\approx 49 \text{ arcmin}^2$) pixels with $\text{res}=9$ resolution scheme (HEALPix, Górski et al. 2005). The SDSS number has been multiplied by 10 to extend the plot range.

6.3 Star–galaxy separation

We noted in §2 that the stellar contamination in our AAΩ–LRG sample could be as high as 16 per cent. Care should therefore be taken when analysing this dataset. We obtained this contamination fraction using the information learned from the AAΩ–LRG spectroscopic survey (Ross et al. 2008, Sawangwit et al. in prep), by imposing a star–galaxy separation in the z -band similar to the method applied in the SDSS- and 2SLAQ–LRG redshift surveys using the i -band. Our optimised star–galaxy separation procedure selects objects with $z_{\text{psf}} - z_{\text{model}} > 0.53 + 0.53(19.0 - z_{\text{model}})$ which only loses genuine LRGs at a sub-percent level and leaves ≈ 16 per cent stellar contamination in our sample, as quoted earlier.

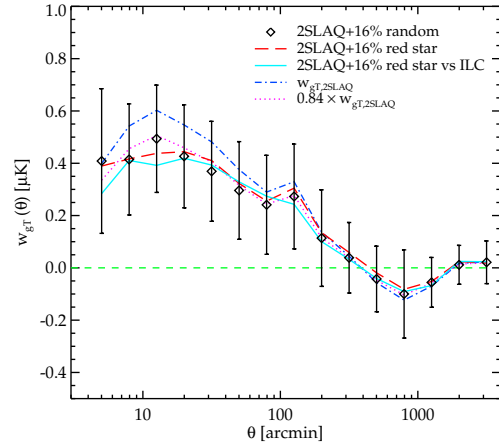


Figure 10. The cross-correlation of the W-band data and the 2SLAQ LRG when a sample of random realisation of ≈ 16 per cent is added to the LRG catalogue (diamonds). The results using original 2SLAQ sample and when multiplied by $1 - f_s$ are shown as the dot-dashed and dotted lines, respectively. The long-dashed line shows the result when the 16 per cent added contaminants are replaced by red stars. The result of cross-correlating the ILC map with the 16 per cent–red star contaminated 2SLAQ sample is also shown (solid line).

The effect of stellar contamination distributed at random in the sample is simply a dilution of the over/under density hence reducing the autocorrelation amplitude of the sample by $(1 - f)^2$ and the cross-correlation by a factor of $(1 - f)$ where f is the fraction of the contamination. This is particularly true if the contamination is distributed uniformly at random in the sample. However, if there is some spatially dependent variation of the number density, a further systematic effect could arise through this process. To test this, we first check to see if there is a trend of the number density as a function of galactic latitude as one might expect for stellar contamination. Although a slight such trend is observed, it is at no more than the levels observed in the SDSS and 2SLAQ samples (see Fig. 9) whose stellar contamination fractions are approximately 1 and 5 per cent, respectively. Next we restrict the data to the high galactic latitude regions, namely $b > 40^\circ$, 50° and 60° . The results are in good agreement with our main results for all three LRG samples up to $b > 60^\circ$ where the cross-correlations become noisy due to the 75 per cent reduction in the sample sizes.

To simulate the effect of the stellar contamination on the LRG–CMB cross-correlation, we have introduced a set of random realisations into the 2SLAQ sample. The result is presented (diamonds) in Fig. 10 along with the cross-correlation of the original 2SLAQ sample (dot-dashed line) and the result of reducing its amplitude by a factor of $(1 - 0.16)$ (dotted line). Furthermore we would like to check for any effects that may arise from possible large scale clustering of the stars. This is done by adding a sample of red stars to the 2SLAQ LRG sample at the 16 per cent level. The stars are selected with similar colour–magnitude criteria to that of the AAΩ LRGs and should mimic the angular distribution and properties of the stellar contaminants seen in the sample. The result is shown in Fig. 10 (long-dashed

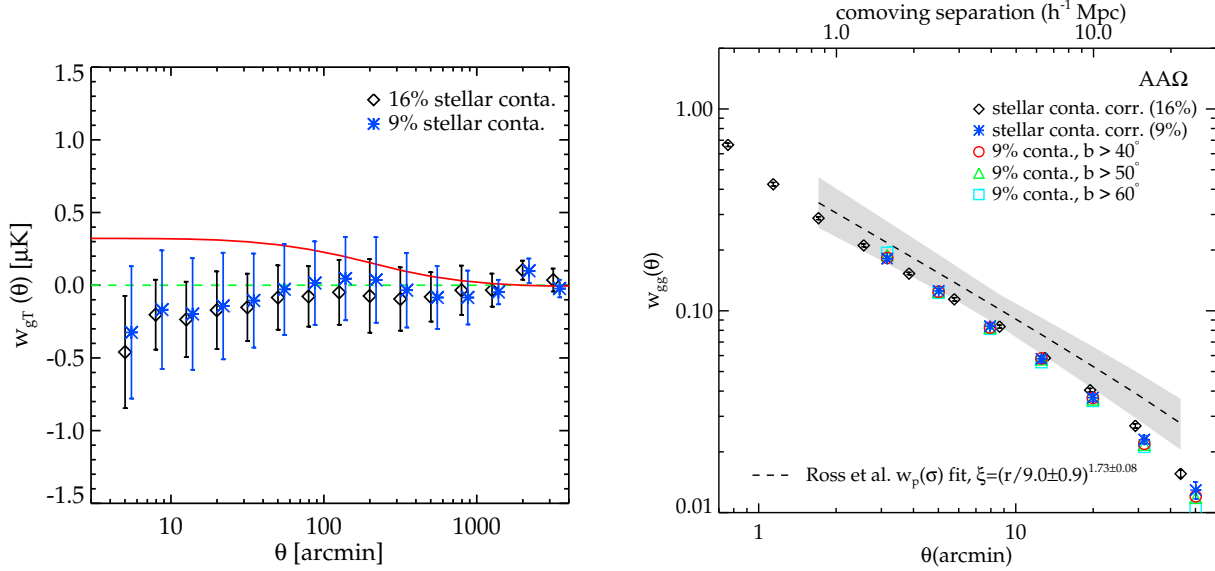


Figure 11. Left: The AA Ω LRG–WMAP5 cross–correlation of the 9% stellar contaminated sample (asterisks) compared to the main AA Ω sample used in our study (diamonds). Right: The corrected autocorrelation functions of the 9%– and 16%–contaminated samples (asterisks and diamonds). These are compared to the results of limiting the 9%–contaminated sample to the regions with galactic latitude higher than $> 40^\circ$, 50° and 60° . The dashed-line and shaded region is the $w_{gg}(\theta)$ and 1σ error inferred from the $w_p(\sigma)$ measured from ≈ 400 spectroscopically confirmed AA Ω LRGs (Ross et al. 2008).

line). This test should also reveal any possible effects on the w_{gT} 's due to (if any) correlation between these stars and the CMB. We found the 16 per cent–red star contaminated 2SLAQ result to be consistent with the dilution of randomly distributed contaminants case. The result is also consistent with the cross–correlation with the foreground reduced ILC map (solid line), further confirming that our result is not affected by any star–CMB cross–correlation. Note that the significance test presented in Table 2 has already taken into account such an effect by multiplying the ISW model by a factor of $(1 - 0.16)$. The significance of the AA Ω sample's rejection of the standard model ISW prediction is therefore robust against the stellar contamination discussed here.

We next attempt to reduce the stellar contamination fraction by imposing a more aggressive star–galaxy separation cut which result in nearly halving the number of genuine AA Ω LRGs. The cut is a combination of the fitted ‘de Vaucouleurs’ radius as a function of z_{deV} magnitude and the correlation between the ‘de Vaucouleurs’ and fiber magnitudes in z -band. This reduces the contamination to ≈ 9 per cent. Fig. 11 (left panel) shows the cross–correlation of this sample with the W -band data which is in good agreement with our main result.

The contamination fractions of these samples are verified by their angular autocorrelation functions, $w_{gg}(\theta)$. The corrected $w_{gg}(\theta)$ is shown in right panel of Fig. 11. This is again in good agreement with the 16 per cent contaminated sample and consistent within $\approx 1\sigma$ of the Ross et al. (2008) power–law fit to the semi–projected correlation function, $w_p(\sigma)$. Note that we only expect the agreement in the range $r \approx 1\text{--}15 h^{-1}$ Mpc where a single power–law is a good fit to the data. The measured w_{gg} 's are also consistent with the results when restricting galactic latitude to greater than 40° , 50° and 60° . We believe the slight discrepancy with the $w_p(\sigma)$ is due to the noisy measurement from the small num-

ber of spectroscopically confirmed LRGs used in Ross et al. (2008) and not caused by the under–estimation of the contamination level as demonstrated by our two independent approaches for star–galaxy separation.

Even if the contamination fraction is under–estimated, the effect of an increased (uniform) stellar contamination would be to increase the ISW model amplitude when the bias value from the LRG autocorrelation is corrected upwards to obtain the true bias value. This upwards shift in the ISW model would then be exactly cancelled by the downwards correction to account for the dilution of the cross–correlation signal due to stellar contamination.

We conclude that despite the faint magnitude limit, and moderate level of stellar contamination (≈ 16 per cent) our ISW results for the AA Ω LRGs seem robust to the tests we have made and the SDSS data seem accurate enough to support this ISW analysis. Up to this point, we have therefore found no explanation in terms of a systematic effect for the low AA Ω –WMAP5 cross–correlation result. Next, we shall perform a similar analysis on some of the large–scale tracers whose ISW effect has been previously claimed in order to test our methodology and look for other possible systematics in these samples.

6.4 SDSS galaxy–WMAP5

We next cross–correlate galaxies extracted from SDSS DR5 using r -band magnitude limits. The objects are photometrically classified as galaxies by the SDSS reduction pipeline. We subsample the galaxies in three magnitude ranges, namely, $18 < r < 19$, $19 < r < 20$ and $20 < r < 21$, where all the magnitudes are galactic extinction corrected model magnitudes. The subsamples contain approximately 2, 6 and 16 millions objects, respectively. This is the same as Cabré et al. (2006, C06 hereafter) but covering ≈ 20 per cent

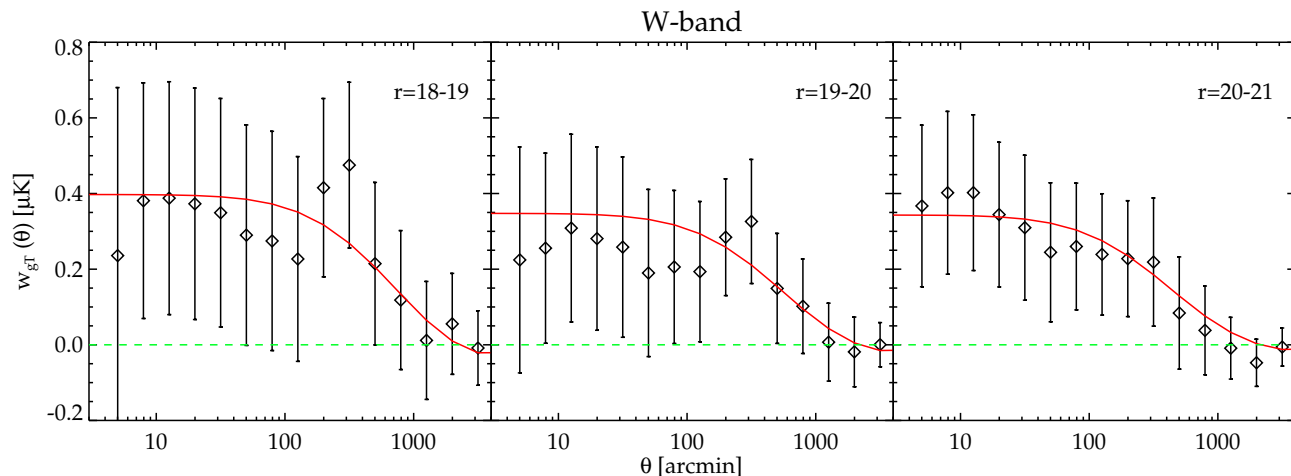


Figure 12. The cross-correlation of *W*-band data with the *r*-band selected galaxies. The sample magnitude ranges are as indicated in the plots. The ISW model prediction is shown for each sample, assuming Dodelson et al. (2002) $n(z)$ with the measured bias of 1.2, 1.1 and 1.2 for $18 < r < 19$, $19 < r < 20$ and $20 < r < 21$ sample, respectively.

more area and we use *WMAP5* rather than *WMAP3*. A similar *r*-band selected galaxy sample was also used by Giannantonio et al. (2008, G08 hereafter) although these authors use ‘ubercalibration’ photometry rather than the original one and limit the sample photo- z to redshift between 0.1–0.9. The ISW effect has been claimed to be detected in these samples at moderate significance level by both C06 and G08 although their results do not agree with the former having twice as much positive cross-correlation between the CMB and the *r*-band selected galaxy sample. As a result C06 need to fit their result with higher Ω_Λ , for a galaxy bias $b = 1.0$.

For the cross-correlation analysis, we proceed in the same manner as with the LRG samples. To compute the ISW model, we use the $n(z)$ distributions following Dodelson et al. (2002). The average redshifts inferred from the $n(z)$ are estimated to be approximately 0.17, 0.24 and 0.33. We then follow our procedure for the LRGs and obtain the galaxy linear bias from the measured amplitude of the galaxy 2-point autocorrelation function for each subsample. We obtain the values $b_g = 1.2, 1.1$ and 1.2 for the sample with *r*-band magnitude limit of 18–19, 19–20 and 20–21, respectively, in agreement with the measurements of C06 and G08 whose $b_g \approx 1$ –1.2. The cross-correlation measurements and the theoretical models are presented in Fig. 12.

We marginally detected the correlation between the CMB data and all the *r*-band selected subsamples. We shall now compare the $20 < r < 21$ result in Fig. 12 to Fig. 2 (top) of C06. Our result is lower by a factor of ≈ 2 but very close to the re-analysis of the SDSS *r*-band data of G08 who also found a factor of two discrepancy with C06. After their discussions, the two groups found that the discrepancy is due to an extra quality-cut imposed on the data by C06, namely, *r*-band magnitude error less than 0.2 mag. We regard the factor of two rise in the amplitude of the cross-correlation after this small change in the magnitude error limit simply as symptomatic of the statistical fragility of the result. We conclude that our re-analyses of these data agree well with the standard Λ CDM predictions although the significance of rejection of the null result is still only ≈ 1 – 2σ .

6.5 NVSS-*WMAP5* cross-correlation

To test our methodology further, we performed a cross-correlation analysis of *WMAP5* with radio sources from the NRAO VLA Sky Survey (NVSS; Condon et al. 1998) which has been previously used by various groups for ISW studies. The NVSS sample comprises about 1.8 million radio sources detected to a flux limit of ≈ 2.5 mJy at 1.4 GHz. The NVSS covers the entire sky higher than -40° declination (≈ 80 percent of the sky). Interestingly, the previous study of Boughn & Crittenden (2002) found no correlation of these sources with the Cosmic Background Explorer (COBE) CMB map but a later study by Nolta et al. (2004) found a positive correlation with the first-year *WMAP* data which they claimed to be the evidence for $\Omega_\Lambda > 0$ at 95% confidence, assuming a flat CDM cosmology. The re-analysis of the NVSS–CMB correlation by G08 also confirmed Nolta et al. (2004) results at approximately the 3σ significance level.

For the cross-correlation analysis we restrict the data to the declination, $\delta \geq -37^\circ$ where the survey is the most complete. We then applied the masking and pixelisation procedure described in §4 but for this sample we shall use lower resolution (res=6 as opposed to res=9) HEALPix Górski et al. (2005) scheme to reduce the computing time because of the much larger sky coverage of the NVSS. We checked that the measurements using different resolutions do give the same results in terms of amplitudes and statistical uncertainties (§6). The higher resolution (res=9) result shall be discussed in this section but for the purpose of the systematics test in §7, we shall present the results using res=6.

Boughn & Crittenden (2002) noticed a number density trend with the declination which affected their autocorrelation measurement. Following Nolta et al. (2004), we applied a correction for this by splitting the sample into $\sin \delta$ strips of width ≈ 0.1 and scaling the galaxy numbers in pixels belonging to a particular strip by the ratio of global mean to the strip mean. The cross-correlation procedure is then carried out as outlined in §4 but the statistical uncertainties and

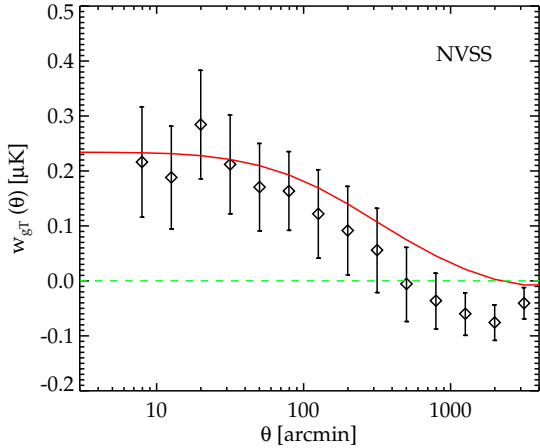


Figure 13. The cross-correlation of the NVSS sources to the W -band data. The ISW prediction (red solid line), assumes linear bias of 1.5 (Boughn & Crittenden 2002; Giannantonio et al. 2008) and $n(z)$ derived from Dunlop & Peacock (1990) radio source luminosity function (mean- z model 1).

covariance matrix are now estimated from approximately 20 equal-area jackknives rather than 24. The result using W -band data along with the standard model ISW prediction (red solid line) is presented in Fig. 13.

The ISW predictions for the NVSS sources are computed using the number-redshift distribution, $n(z)$, derived from the radio source luminosity function (mean- z model 1) of Dunlop & Peacock (1990). The median redshift estimated from such $n(z)$ is ≈ 0.8 with a tail extending out to $z \approx 3$. We assume the source bias, b , of 1.5 as measured by a number of authors (e.g. Boughn & Crittenden 2002; Giannantonio et al. 2008).

Fig. 13 shows that we find a marginally positive correlation similar to the prediction of the standard model at scales smaller than $\approx 5^\circ$ at $\approx 2\sigma$ significance. Our result can be directly compared with that of G08 who, like us, cross-correlate the source number fluctuations to Δ_T as opposed to the source number per pixel approach of Nolta et al. (2004). Similarly, G08 observed a good agreement between their measurement and the standard Λ CDM model which also starts to breakdown at $\approx 5^\circ$. We take this agreement as a further indication of the robustness of our cross-correlation methodology and analyses. In the next section, we shall further test the NVSS- $WMAP5$ result for contamination by systematic effects.

7 CMB SKY ROTATION TEST

Here we shall perform an additional test for systematics, similar to that used by Myers et al. (2004) and Bielby & Shanks (2007) for testing their detection of the SZ effect, particularly in checking the reality of a large scale temperature decrement around galaxy groups and clusters. We follow these authors and rotate the $WMAP$ maps around the galactic pole in the clockwise direction, each time adding 40° to galactic l . There is an area very close to the pole where there is less movement from the rotation, but given that we

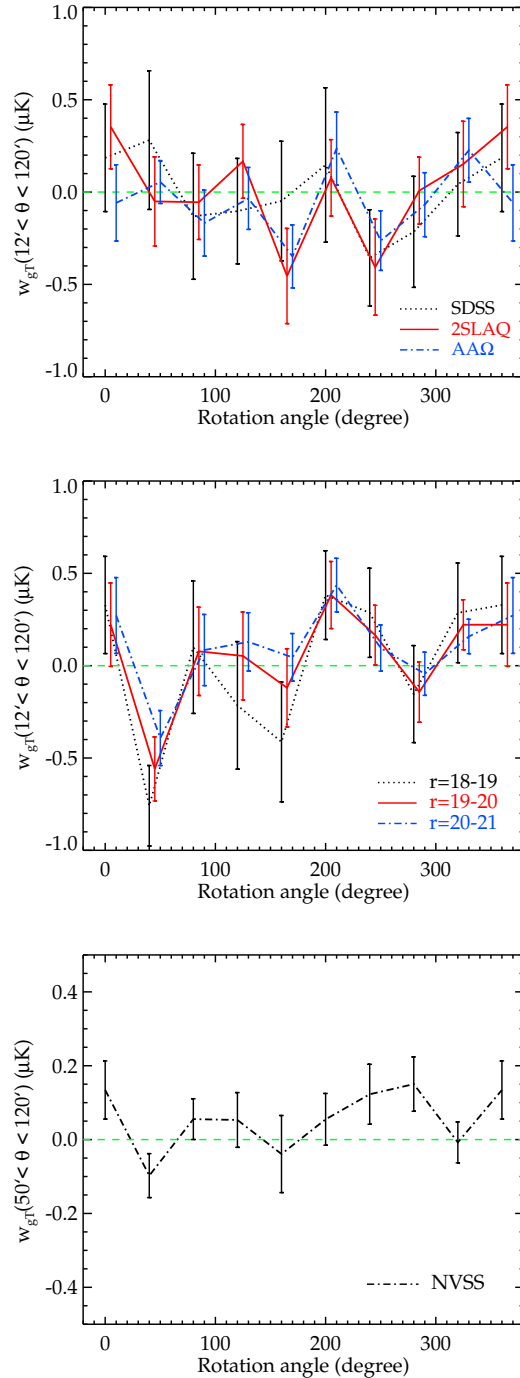


Figure 14. The cross-correlation of the three LRG samples (top), r -band selected galaxies (middle) and the NVSS sources (bottom) to the rotated W -band data in our rotation test (see text for more details). Note that for the top two plots, the points have been shifted slightly in the x-axis for clarity.

use a 40° shift the effect of this slight non-independence is small. We have checked that if we cut out the circum-polar region down to galactic latitude $b = 75^\circ$ our results are unaffected.

The CMB masks (KQ75 plus point source) are rotated with the temperature maps to ensure that the contaminated

regions are excluded from both galaxy and temperature fluctuation maps. The SDSS DR5 mask is then applied to the data in the case of LRG and r -band selected samples. The cross-correlation is performed using the W -band data following the procedure described in §4. We use the cross-correlation results between $12' < \theta < 120'$ where the difference between the ISW and null result is at its maximum as in §5. The cross-correlations are then performed at eight 40° intervals.

7.1 LRGs

The cross-correlation measurements are presented in Fig. 14 (top panel). The errors shown are jackknife errors (1σ) and as expected they are similar at all rotation angles which makes the data points straightforward to compare. For the SDSS sample at $z=0.35$, there is a higher positive point at rotation angle 40 degrees. For the 2SLAQ sample at $z=0.55$ the points at rotation angles 160 and 240 degrees are more negative than the zero degree point is positive. There is no reason to expect anything other than a null result at any rotation angle other than zero. Therefore, based on this rotation test the significances are now reduced to the $\approx 12-25\%$ level, suggesting that systematics as well as statistical errors may be affecting the data.

7.2 SDSS galaxies

We also applied the same test to the ISW results using three SDSS r -band selected galaxy samples of $18 < r < 19$, $19 < r < 20$ and $20 < r < 21$. The results are shown in Fig. 14 (middle). Again we see that there are rotation angles that show more significant non-zero detections than at the zero degree rotation angle. We see that at 40° rotation angle, the results are very negative in all three samples. At the rotation angle of 200° , the results are more positive than the zero degree rotation, again in all three samples. As for the LRG samples, this means that the significance is reduced to a marginal $\approx 10\%$ level and the results suggest that systematic effects as well as statistical errors may be contributing to the apparent ISW detection at zero degrees rotation angle.

7.3 NVSS radio sources

We then applied the same test to the NVSS–*WMAP5* cross-correlation result. (see Fig. 14, bottom). This time the point at rotation angle 280 degrees is more positive than the point at zero degrees. As with other samples, the jackknife errors on all the points are similar so this comparison is fair. Again we conclude that systematic effects may be contributing to the apparent ISW detection which explains the reduction in statistical significance to $> 10\%$ from the rotation test.

8 DISCUSSION

Given the consistency of the $\Lambda\Omega$ and the combined LRG results with the zero correlation, we now discuss whether there is any contradiction between our conclusions and those of other authors. In particular, we discuss the results of G08 who claim a 4.5σ ISW detection from the combined analyses of several large-scale tracers. These tracers include some of

the LRG samples. They also include NVSS radio sources. The most significant detection in their Table 1 is from the NVSS at 3.3σ . Their LRG analysis gives 2.2σ for a sample roughly equivalent to our 2SLAQ LRG sample. These compare to 1.6σ for our 2SLAQ samples. For the NVSS we find a 1.8σ result. Their SDSS galaxy sample gives 2.2σ equivalent to our combined SDSS r -band limited sample which gives $\approx 1.3\sigma$ significance. Thus our significances appear lower than those of G08, particularly for NVSS. This discrepancy increases when we consider the rotation test. In the rotation test of the NVSS sample, 1 out of 8 points has higher amplitude than zero rotation measurement which is only $\approx 1.5\sigma$ significance. For the 2SLAQ case, this gives 1–2 out of 8 points which is equivalent to $1.2-1.5\sigma$ significance. The SDSS galaxy gives 2 higher (or lower) points in 8 or $\approx 1.2\sigma$.

However, G08 also have differences between their two methods of assessing the significance of their results. Their Table 1 assumes the hypothesis of the standard Λ CDM model to obtain a maximum likelihood amplitude, A , and an associated error from their data. This error is different from the error that can be inferred from the χ^2 statistic in their Table 2 which tests the null result hypothesis. For example, their LRG result is 0.4σ significant from Table 2 whereas it is 2.2σ significant from Table 1. Their SDSS galaxy sample rejects the null result hypothesis at 1.3σ significance from the χ^2 statistic, again lower than their Table 1 at 2.2σ . Also the NVSS only reject the null result at 1.3σ rather than 3.3σ . We assume that these differences may be due partly to different null hypotheses and partly due to different methodologies. Certainly, the levels of significance in their Table 2 are lower and more in line with what our rotation tests show, i.e. 1–2 higher (or lower) points in 8 or $1.2-1.5\sigma$. It remains to be seen for the other samples in their Table 1 and 2, if the same pattern applies with the maximum likelihood significances in Table 1 being higher than the χ^2 significances in Table 2. We conclude that the rejection of the null result by their χ^2 test may be more consistent with what we have found than the results in their Table 1. Indeed their χ^2 summed from all surveys is 67 on 74 degrees of freedom which is hardly a significant rejection of the null result and can be compared to our overall rejection of the null result in our Table 2 of 0.5 to 1σ . Therefore as long as we refer to the χ^2 test of G08, there seems to be no inconsistency with our estimate of the significance of the low rejection of the null result.

9 SUMMARY AND CONCLUSION

We have performed a cross-correlation analysis between the *WMAP5* CMB data and various large-scale structure tracers including our new high redshift $\Lambda\Omega$ -LRG survey. The summarised conclusions of our findings are as follows:

- We have found a null ISW result for $z \approx 0.7$ $\Lambda\Omega$ -LRG sample. The standard model is rejected at $\approx 3\%$ significance by this dataset.
- We have confirmed the marginal correlations between *WMAP5* CMB temperature fluctuations and SDSS LRGs at $z=0.35$ and 2SLAQ LRGs at $z=0.55$.
- The null result in the $\Lambda\Omega$ -LRG sample at large scales is unlikely to be caused by the negative contribution of the

SZ effect, given its angular extent and the expected amplitude of ISW signal.

- We have made a range of tests on the $\text{AA}\Omega$ cross-correlation measurement which confirms its robustness. These include moving the magnitude limits up to 0.5mag brighter, removing areas of sky with significant dust absorption, using an estimate of the cross-correlation that takes out any possible systematic effects due to SDSS stripes and comparing the standard and uber-calibrations of the SDSS photometry. We have also checked the effects of stellar contamination in our samples. All these tests produce results consistent with our original measurements.

- We have also reproduced the cross-correlation results of most previous authors using our techniques. In particular we have reproduced the marginally positive correlations seen using SDSS magnitude limited samples of galaxies and NVSS radio sources.

- However, rotation tests indicate that accidental alignment or some unknown systematics can give rise to a correlation signal comparable to and in many cases even larger than the ISW signal itself. This suggests that the previous positive detections may still be subject to unknown systematic effects.

- Combining the new $\bar{z} \approx 0.7$ LRG survey with the lower redshift LRG samples, the overall cross-correlation result is now as consistent with a null detection as it is with the standard Λ CDM model for both W -band and ILC data. For the ILC map, the significance of rejecting the standard model is $\approx 2\sigma$ whereas the result is only 0.5σ away from the zero correlation hypothesis.

- Given the results of the rotation test on the SDSS and 2SLAQ LRG samples, the support these give to the standard ISW model in the combined sample may have even less statistical weight than indicated above.

- There is a possibility that the absence of the ISW correlation in the high redshift dataset is due to evolution of the dark energy equation of state. However, we regard it as unlikely that evolution could take place over the short redshift interval between the 2SLAQ and $\text{AA}\Omega$ datasets. It is more plausible that the differences between the redshift bins are purely statistical, particularly given the rotation test results. We note that the individual positive detections that we have discussed are only marginally statistically significant and the combined ILC dataset is more consistent with zero than with the standard model prediction.

- If the ISW effect was generally absent then the impact on cosmology would be large because this would be strong evidence against an accelerating Universe. This would therefore argue against a significant role for a cosmological constant or dark energy in the Universe. Moreover, the absence of ISW would also argue against any modified gravity model which produced acceleration. The model which would be heavily favoured would be an Einstein-de Sitter model with $\Omega_m = 1$. However, if such a model had a critical density of exotic, CDM particles then there might be a contradiction with the high baryon densities in rich galaxy clusters such as Coma. This rich cluster ‘baryon catastrophe’ has previously argued against a high CDM density because starting from $\Omega_b/\Omega_m \approx 0.03$, it was difficult to understand in a hierarchical model how to produce a $5\times$ bigger baryon fraction in rich galaxy clusters (White et al. 1993).

- It is therefore important to repeat the LRG measure-

ments made here, now in the Southern sky. One opportunity to do this will arise from the new ESO imaging surveys in the South which are about to start, the VST ATLAS and the VISTA Hemisphere Survey. If the results we have found here are repeated then there could be significant consequences for cosmology.

ACKNOWLEDGEMENTS

US acknowledges financial support from the Institute for the Promotion of Teaching Science and Technology (IPST) of The Royal Thai Government. We thank Douglas Scott for useful discussion and comments. We thank all the present and former staff of the Anglo–Australian Observatory for their work in building and operating the 2dF and $\text{AA}\Omega$ facility.

Funding for the SDSS and SDSS-II has been provided by the Alfred P. Sloan Foundation, the Participating Institutions, the National Science Foundation, the U.S. Department of Energy, the National Aeronautics and Space Administration, the Japanese Monbukagakusho, the Max Planck Society, and the Higher Education Funding Council for England. The SDSS Web Site is <http://www.sdss.org/>.

The SDSS is managed by the Astrophysical Research Consortium for the Participating Institutions. The Participating Institutions are the American Museum of Natural History, Astrophysical Institute Potsdam, University of Basel, Cambridge University, Case Western Reserve University, University of Chicago, Drexel University, Fermilab, the Institute for Advanced Study, the Japan Participation Group, Johns Hopkins University, the Joint Institute for Nuclear Astrophysics, the Kavli Institute for Particle Astrophysics and Cosmology, the Korean Scientist Group, the Chinese Academy of Sciences (LAMOST), Los Alamos National Laboratory, the Max-Planck-Institute for Astronomy (MPIA), the Max-Planck-Institute for Astrophysics (MPA), New Mexico State University, Ohio State University, University of Pittsburgh, University of Portsmouth, Princeton University, the United States Naval Observatory, and the University of Washington.

REFERENCES

- Abazajian K. N., et al. 2009, *ApJS*, 182, 543
 Adelman-McCarthy J. K., et al. 2007, *ApJS*
 Afshordi N., Loh Y.-S., Strauss M. A., 2004, *Phys. Rev. D*, 69, 083524
 Bielby R. M., Shanks T., 2007, *MNRAS*, 382, 1196
 Boughn S., Crittenden R., 2004, *Nature*, 427, 45
 Boughn S. P., Crittenden R. G., 2002, *Physical Review Letters*, 88, 021302
 Cabré A., Gaztañaga E., Manera M., Fosalba P., Castander F., 2006, *MNRAS*, 372, L23
 Cannon R., et al. 2006, *MNRAS*, 372, 425
 Carroll S. M., 2001, *Living Reviews in Relativity*, 4, 1
 Carroll S. M., Press W. H., Turner E. L., 1992, *ARA&A*, 30, 499
 Cole S., et al. 2005, *MNRAS*, 362, 505
 Collister A., et al. 2007, *MNRAS*, 375, 68

- Condon J. J., Cotton W. D., Greisen E. W., Yin Q. F., Perley R. A., Taylor G. B., Broderick J. J., 1998, *AJ*, 115, 1693
- Crittenden R. G., Turok N., 1996, *Physical Review Letters*, 76, 575
- Dodelson S., et al. 2002, *ApJ*, 572, 140
- Douspis M., Castro P. G., Caprini C., Aghanim N., 2008, *A&A*, 485, 395
- Dunkley J., et al. 2009, *ApJS*, 180, 306
- Dunlop J. S., Peacock J. A., 1990, *MNRAS*, 247, 19
- Eisenstein D. J., et al. 2001, *AJ*, 122, 2267
- Eisenstein D. J., Hu W., 1998, *ApJ*, 496, 605
- Fosalba P., Gaztañaga E., Castander F. J., 2003, *ApJ*, 597, L89
- Giannantonio T., Scranton R., Crittenden R. G., Nichol R. C., Boughn S. P., Myers A. D., Richards G. T., 2008, *Phys. Rev. D*, 77, 123520
- Gold B., et al. 2009, *ApJS*, 180, 265
- Górski K. M., Hivon E., Banday A. J., Wandelt B. D., Hansen F. K., Reinecke M., Bartelmann M., 2005, *ApJ*, 622, 759
- Granett B. R., Neyrinck M. C., Szapudi I., 2008, *ApJ*, 683, L99
- Hinshaw G., et al. 2009, *ApJS*, 180, 225
- Ho S., Hirata C., Padmanabhan N., Seljak U., Bahcall N., 2008, *Phys. Rev. D*, 78, 043519
- Hu W., Scranton R., 2004, *Phys. Rev. D*, 70, 123002
- Jarrett T. H., Chester T., Cutri R., Schneider S., Skrutskie M., Huchra J. P., 2000, *AJ*, 119, 2498
- Limber D. N., 1953, *ApJ*, 117, 134
- Limon M., et al. 2008, available in electronic form at <http://lambda.gsfc.nasa.gov>
- McEwen J. D., Vielva P., Hobson M. P., Martínez-González E., Lasenby A. N., 2007, *MNRAS*, 376, 1211
- Metcalf N., Shanks T., Campos A., McCracken H. J., Fong R., 2001, *MNRAS*, 323, 795
- Myers A. D., Shanks T., Outram P. J., Frith W. J., Wolfendale A. W., 2004, *MNRAS*, 347, L67
- Nolta M. R., Wright E. L., Page L., Bennett C. L., Halpern M., Hinshaw G., Jarosik N., Kogut A., Limon M., Meyer S. S., Spergel D. N., Tucker G. S., Wollack E., 2004, *ApJ*, 608, 10
- Padmanabhan N., et al. 2007, *MNRAS*, 378, 852
- Padmanabhan N., et al. 2008, *ApJ*, 674, 1217
- Padmanabhan N., Hirata C. M., Seljak U., Schlegel D. J., Brinkmann J., Schneider D. P., 2005, *Phys. Rev. D*, 72, 043525
- Peebles P. J., Ratra B., 2003, *Reviews of Modern Physics*, 75, 559
- Peebles P. J. E., 1980, *The large-scale structure of the universe*. Princeton University Press
- Perlmutter S., et al. 1999, *ApJ*, 517, 565
- Riess A. G., et al. 2007, *ApJ*, 659, 98
- Ross N. P., et al. 2007, *MNRAS*, 381, 573
- Ross N. P., Shanks T., Cannon R. D., Wake D. A., Sharp R. G., Croom S. M., Peacock J. A., 2008, *MNRAS*, 387, 1323
- Sachs R. K., Wolfe A. M., 1967, *ApJ*, 147, 73
- Scharf C., Hoffman Y., Lahav O., Lynden-Bell D., 1992, *MNRAS*, 256, 229
- Schlegel D. J., Finkbeiner D. P., Davis M., 1998, *ApJ*, 500, 525
- Scranton R., et al. 2003, *ArXiv Astrophysics e-prints*
- Sunyaev R. A., Zeldovich I. B., 1980, *ARA&A*, 18, 537
- Tegmark M., et al. 2006, *Phys. Rev. D*, 74, 123507
- Wake D. A., et al. 2008, *MNRAS*, 387, 1045
- White S. D. M., Navarro J. F., Evrard A. E., Frenk C. S., 1993, *Nature*, 366, 429
- Wright E. L., et al. 2009, *ApJS*, 180, 283